DISSERTATIONES
SCIENTIAE
MATERIALIS
UNIVERSITATIS
TARTUENSIS
26

SIIM HÖDEMANN

Residual stress determination in chemically strengthened and thermally tempered glass plates using scattered light method

DISSERTATIONES SCIENTIAE MATERIALIS UNIVERSITATIS TARTUENSIS
26

DISSERTATIONES SCIENTIAE MATERIALIS UNIVERSITATIS TARTUENSIS
26

SIIM HÖDEMANN

Residual stress determination in chemically strengthened and thermally tempered glass plates using scattered light method

UNIVERSITY OF TARTU
Press

This study was carried out at the University of Tartu, Institute of Physics.

The Dissertation was admitted on January 23, 2019, in partial fulfillment of the requirements for the degree of Doctor of Philosophy in Materials Science, and allowed for defense by the Council of Materials Science of the University of Tartu.

Supervisors: Prof. Jaak Kikas, University of Tartu, Estonia

Assistant Prof. Eric R. Tkaczyk, Vanderbilt University Medical Center and Vanderbilt University, USA

Opponent: Prof. Vincenzo M. Sglavo, Department of Materials Science and Technology, University of Trento, Italy

Defense: March 1, 2019

This work has been partially supported by the graduate school "Functional materials and technologies", receiving funding from the European Social Fund under project 1.2.0401.09-0079 in Estonia, Estonian Enterprise research projects and GlasStress Ltd.

ISSN 2228-0928
ISBN 978-9949-77-975-8 (print)
ISBN 978-9949-77-976-5 (pdf)

University of Tartu Press
www.tyk.ee

CONTENTS

LIST OF ORIGINAL PUBLICATIONS

This thesis is based on the following publications (full texts included at the end of the thesis), which are referred to in the text by their Roman numerals.

I H. Aben, J. Anton, A. Errapart, S. Hödemann, J. Kikas, H. Klaassen and Marko Lamp. "On non-destructive residual stress measurement in glass panels," *Estonian Journal of Engineering*, **16**(2):150–156 (2010)

II J. Anton, A. Errapart, M. Paemurru, Dominique Lochegnies, Siim Hödemann and H. Aben. "On the inhomogeneity of residual stresses in tempered glass panels," *Estonian Journal of Engineering* **18**(1):3–11 (2012)

III S. Hödemann, P. Möls, J. Kikas and J. Anton. "Scattered laser light fringe patterns for stress profile measurement in tempered glass plates," *Glass Technology: European Journal of Glass Science and Technology* **55**(3):90–95 (2014)

IV S. Hödemann, P. Möls, V. Kiisk, T. Murata, R. Saar, J. Kikas. "Confocal detection of Rayleigh scattering for residual stress measurement in chemically tempered glass," *Journal of Applied Physics* **118**:243103 (2015)

V S. Hödemann, A. Valdmann, J. Anton, T. Murata. "Gradient scattered light method for non-destructive stress profile determination in chemically strengthened glass," *Journal of Materials Science* **51**:5962–78 (2016)

VI S. Hödemann, A. Valdmann, V. Kiisk. "An iterative approach to remove the influence of light ray bending from micron-scale scattered light tomography," *Optics and Lasers in Engineering* **91**:30–40 (2017)

AUTHOR'S CONTRIBUTION

I Performing destructive testing and SCALP measurements. Preparing Figure 4.

II Discussions.

III Performing all measurements, analyzing the data, writing of the article. Preparing graphs, except Figure 1.

IV Developing the stress measurement method. Performing experiments, data analysis and writing the article except the description of the construction of confocal microscope and the calculation of axial and lateral resolution. Preparing graphs, except Figure 1.

V Participating in development of algorithm that removes the influence of light ray bending from oblique incidence scattered light method. All graphs, all other writing than the description of ray tracing. Co-authors carried out all experiments and developed experimental apparatus.

VI Testing the algorithm (from previous paper) that removes the influence of light ray bending from oblique incidence scattered light method in case of stress profiles from literature. All graphs, all other writing than the description of ray tracing.

ABBREVIATIONS AND SYMBOLS

e-ray	extraordinary ray
o-ray	ordinary ray
δ	optical retardation (path length difference between the e-ray and o-ray)
$\delta_c(y)$	optical retardation along curved ray path
$\delta_s(y)$	optical retardation along straight ray path
C	stress-optic coefficient (photoelastic coefficient)
C_1, C_2	absolute stress-optic coefficients
SRI	straight ray inversion
CRI	curved ray inversion
CRID	curved ray inversion that removes the reconstruction errors caused by the influence of compositionally induced refractive indices
$\sigma_{sri}(y)$	stress profile calculated by using SRI
$\sigma_{cri}(y)$	stress profile calculated by using CRI
σ_{surf}	surface stress
n_b	refractive index of glass substrate (core)
$n_u(y)$	depth dependence of refractive index of unstressed glass (contains compositional component)
n_{prism}	refractive index of glass prism
α	incidence angle in glass prism
LAS	lithium aluminosilicate glass
NAS	sodium aluminosilicate glass
DOL	depth of compressive stress layer (case-depth)
MOR	modulus of rupture (bending strength. flexure strength)
EDX	energy dispersive X-ray
GRIN	gradient index

1 INTRODUCTION

1.1 Correlation between internal residual stresses and overall strength of glass plate

The fundamental purpose of both thermal tempering and chemical strengthening is to create compressive stresses near the surface. The physical pressure thus altered at the surface adds a substantially higher tensile stress requirement to the external forces required to grow cracks. Similarly, the resistance to abrasions is also increased. Effectively, glass becomes much stronger. Strengthening is carried out at temperatures below glass transition temperatures to avoid/reduce stress relaxation.

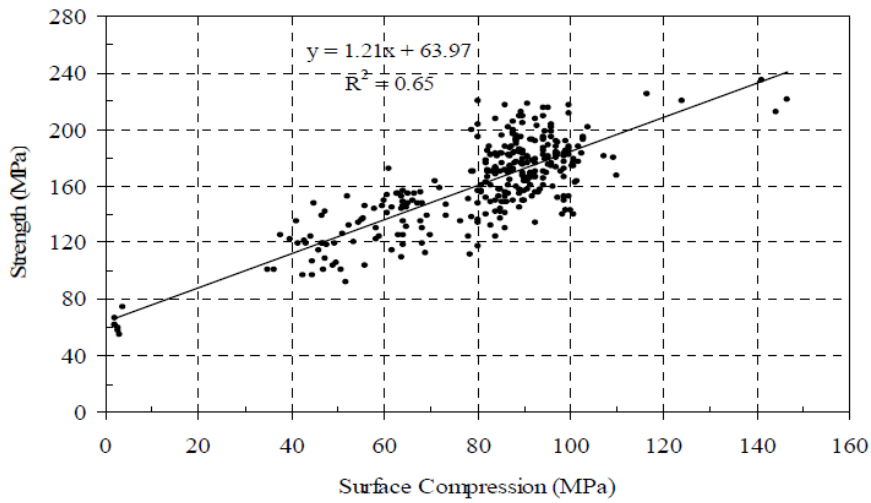

Figure 1.1 Relationship between the surface compressive stress and breaking strength of thermally tempered glass plates (GPD 2005 [1]).

Figure 1.1 shows correlation between surface stresses measured with **g**razing **a**ngle **s**tress **p**olariscope GASP (StrainOptics Inc., USA) and bending strength. GASP can measure stress at tin side only because the refractive index is then high enough for several successive curved refracted rays to resurge. Authors concluded that a good correlation has been observed between surface compressive stress data and mechanical strength measured according to standardized 4-point bending test. This correlation is higher when both measurements are carried out on the same side and on uncoated float glass specimens. Similar results have been obtained by several other authors [2–3].

1.2 Overview of evolution of scattered light method for stress measurement in tempered glass plates

James Clerk Maxwell predicted the possibility of scattered light method already in 1853 [4], but was experimentally discovered by Weller in 1941[5]. The scattered light method can be used to measure the stress profile measurement in thermally tempered glass plates. Note that transmitted light can only be used for edge stress measurement of glass plates. Although there is some correlation between edge stresses and surface stresses [6], it is impossible to retrieve precise surface stresses from edge stress measurement results. Bateson *et al*. [7] introduced laser as a light source for the method.

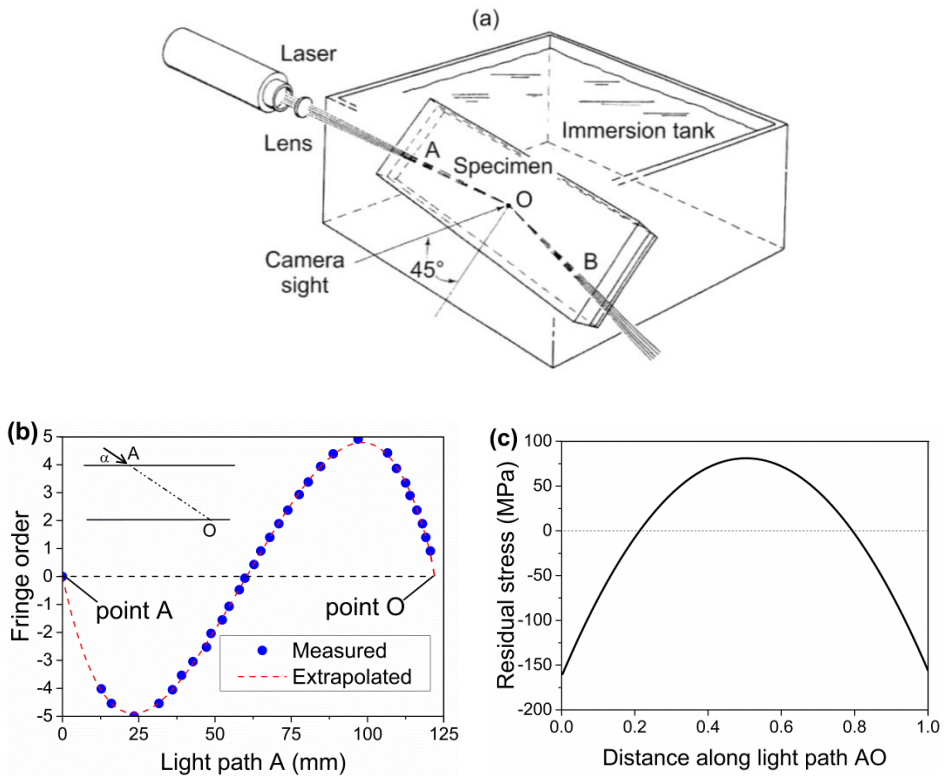

Figure 1.2 Cheng's original experimental setup for scattered-light method to determine stress profile in thermally tempered glass plate. **(a)** Experimental setup; **(b)** measured fringe order along light ray path; **(c)** Residual stress along light path (here and in this thesis compressive stresses have negative values). (Cheng [8]).

In early studies stresses were calculated directly from Rayleigh scattered light fringe patterns (by detecting spatial modulation periods of scattered light intensity). Figure 1.2 shows Cheng's measurement setup, where monochromatic

linearly polarized light is passed through glass plate at incidence angles of 82° and 84°. Such high incidence angles increase the number of full fringes viewable. Compensator or wave-plates were not used in this setup. Glass plate under study was in immersion oil, to eliminate refraction at point A. Camera sight was at 45° to glass surface for ensuring maximum fringe visibility. Stress profile was calculated from fringe order, which itself in turn is calculated from the maximum or minimum intensity fringe positions.

Cheng also proposed the dual-observation scattered light method [9]. The scattered light intensities are recorded simultaneously along two directions of observation. This gives same effect as a compensator with fixed position is used. Both fringe patterns can be used to calculate stresses, thus enabling somewhat more precise measurement of stress profile.

Many authors pointed out problems of recording and interpretation of the scattered light fringes [7–8, 10–11]. Consequently, the phase modulation method was introduced by Colombotto *et al.* [12] after recognizing that the optical retardation resulting from the birefringence can be evaluated by modulating the polarization state of incident light. This way, scattered light intensity at each point along the light beam is modulated at a suitable constant frequency. Hence, the Cheng's classical method of inspecting fringe patterns by CCD camera could be replaced to form the basis for an automatic measuring system.

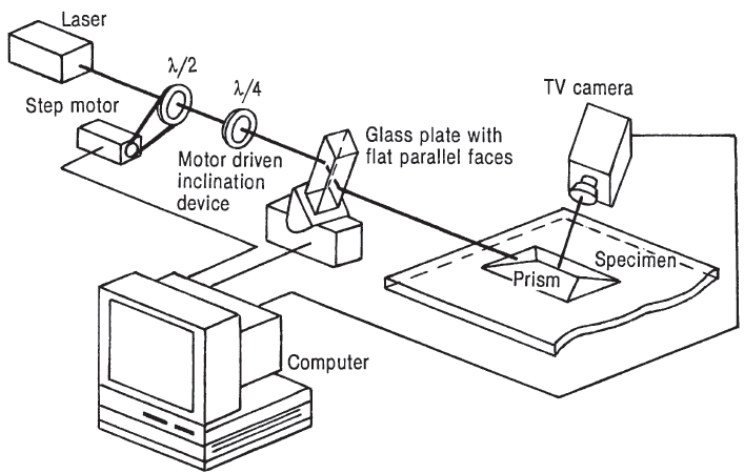

Figure 1.3 Weißmann & Dürkop's original setup to measure the phase shift of scattered light in a tempered glass plate. (Weißmann & Dürkop [13])

Figure 1.3 shows setup used by Weißmann & Dürkop to automatically measure stress profile. Phase shift and the corresponding stress distribution through the thickness of a tempered glass plate, assuming a uniform strengthening from

both surfaces, which results in symmetric close-to-parabolic stress profile. Light from helium-neon laser was first modulated by means of a rotating half-wave plate and then passed through a fixed quarter wave plate before passing through a coupling prism into the test sample.

Basic concept of phase modulation method with the use of wave-plates (compensator can be used for the same purpose) is as follows: After linearly polarized incident light passes through the λ/4-plate the polarization state of the light (elliptically, circularly or linearly polarized) is controlled by the angle between the optic axis of the λ/4-plate and the direction of the polarization plane of the incident light. Therefore the rotation angle of the λ/2-plate directly determines the polarization state of the light that comes out from the λ/4-plate. Figure 1.4 illustrates that by rotating the λ/2-plate, the scattered light intensity begins to modulate in depending on the rotation angle of the plate. By measuring the dependence of the scattered light intensity on the rotational angle of the plate φ for two spatially close points x_1 and x_2, one obtains two sinusoids with a phase difference Δ, which in turn gives the residual stress:

$$\sigma_1 - \sigma_3 = \frac{\Delta \cdot \lambda}{2\pi \cdot C \cdot \Delta x}, \quad (1.1)$$

where Δx is the distance between x_1 and x_2, λ is wavelength of light and C is stress-optic coefficient of glass in Brewsters (Br). For example, one option to determine C is to use automatic birefringence measurement device ABR-10A-EX (Uniopt Ltd., Japan). Another option for same measurement is to use an **a**utomatic **p**olariscope AP-07 (GlasStress Ltd., Estonia). The disc-shaped samples are prepared and a load is applied diametrically, and the corresponding change in the optical retardation is measured.

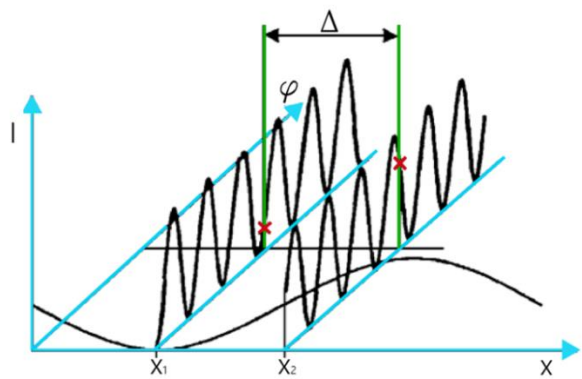

Figure 1.4 Phase modulation method: measurement of phase shift of the scattered light intensity allows the stress to be determined. Light propagates along the direction of x-axis. We observe that by rotating λ/4-plate by angle φ scattered light intensity modulation starts spatially moving. Therefore scattered light intensity modulation can be observed at each point along the light ray.

The scattered-light technique was further developed by Shepard *et al*. [14] to measure wider range of residual stresses (including those of low magnitude) across the thickness of flat and moderately curved glass products, utilizing modern digital imaging equipment to substantially improve monitoring efficiency. The general experimental arrangement was similar to that adopted by Weißmann & Dürkop [13], but included a compensator instead of a set of fixed and rotating wave-plate. Anton [15] developed compact polariscope based on oblique incidence scattered light method for stress profile measurement in tempered glass plates. Tennakoon [16] developed a polariscope that is based on detecting fluorescence instead of directly detecting Rayleigh scattering. However, the same e-ray and o-ray that induce Rayleigh scattering are also inducing fluorescence, so therefore this method is also basically another version of scattered light method.

1.3 Compensating (removing) the influence of light ray bending

For strongly refractive media such as chemically tempered glasses where the component of the refractive index gradient ∇n is perpendicular to the propagation direction of the light beam, the straight ray inversion can lead to significant reconstruction errors; therefore, inversion schemes must be developed to include refraction correction.

Consequently, reconstruction algorithms have been developed to compensate the influence of the bending of light rays. In numerical experiments where these algorithms were applied to optical retardation profiles numerically generated from a known stress field, iterations often departed from the known field after approaching the reference solution first. Dolovich *et al.* [17] described an iterative approach to remove the influence of light ray bending from transmission photoelasticity. Dolovich & Gladwell [18] tested iterative schemes for reconstructing refractive-index fields to establish sufficient conditions for convergence. Lira & Vest [19] reviewed iterative approaches, intended for refractive index reconstruction, for which convergence is not guaranteed. Acosta *et al.* [20] presented an iterative tomographic algorithm for the reconstruction of refractive-index profiles for fiber preforms and GRIN lenses from the measured deflection angles of refracted light beams.

All other previous studies on the influence of light ray bending in residual stress tomography focused on the photoelasticity of transmitted light. Initial studies on the light ray bending influence in transmitted light photoelasticity were carried out by Bokshtein [21]. Hecken & Pindera [22] and Aben *et al.* [23] proposed to integrate the experimentally measured deflections of light rays into the photoelastic theory. Pagnotta & Poggialini [25] also used Aben's concept of experimental measurement of the light beam deflections to compensate the influence of light ray bending in transmission photoelasticity in residual stress measurement in axially symmetric fiber preforms. They used experimentally

measured radial refractive index profiles instead than Maxwell's stress-optic equations that were reported by Dolovich *et al.* [17]. The fiber was scanned with a He-Ne laser and the deflections of the laser beam were analyzed to determine the radial refractive index profile. The authors described experimental and computational results (optical retardations along the curved ray path and straight ray path).

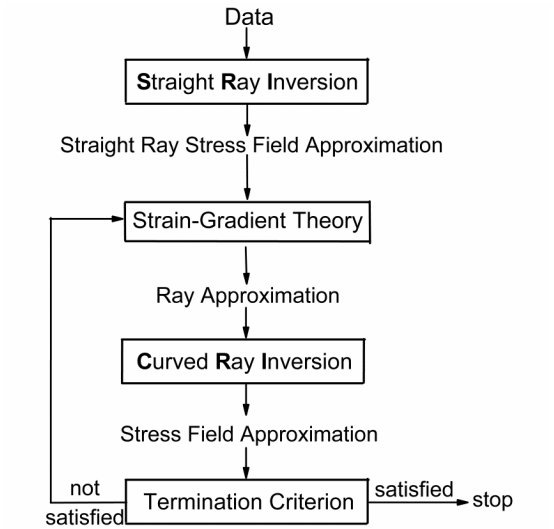

Figure 1.5 Dolovich's iterative scheme for curved-ray data analysis. It is based on similar versions of this scheme used before by other authors. (Dolovich *et al.* [17])

Figure 1.6 shows Acloque & Guillemet's stress measured method based on measuring optical retardation shift due to on light ray bending (transmitted light gradient photoelasticity [25]). Bending of light rays might be a source of error in photoelastic tomography. But parabolic stress profile can be calculated from refraction-induced optical retardation. However, this method is limited to stress profiles of known shapes, for example, a near-parabolic stress profile in thermally tempered glass plate. The exact shape of the stress profile in thermally tempered glass plate can be described by the theory of Narayanaswamy [27] or Indenbom [26]. Stress profiles in chemically strengthened glass plates can have engineered shapes [28], which can't be measurable by the transmitted light gradient photoelasticity.

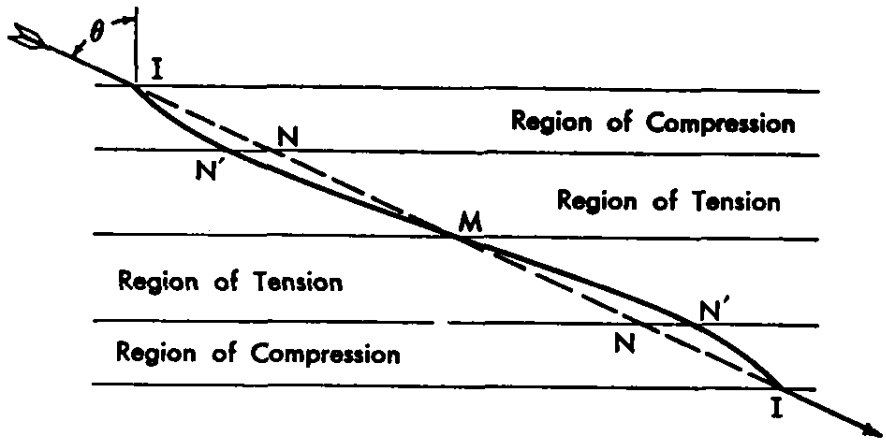

Figure 1.6 Concept of transmitted light gradient photoelasticity stress measurement method**:** Light ray passing obliquely through a thermally tempered glass plate. In actual experiment light ray passes through plate along N' but in rectilinear model assumed to pass along N. (Acloque & Guillemet [26]).

1.4 Chemically strengthened lithium aluminosilicate glass

Chemically strengthened aluminosilicate glass, which has high impact and scratch resistance, has been used as a protective cover for space solar panels [29], mobile devices [30] and mirror foil for future X-ray telescopes [31]. Note that case-depth for aluminosilicate strengthened by $K^+ \leftrightarrow Na^+$ ion-exchange is limited to ~50 μm. Chemically strengthened lithium aluminosilicate glass can be ion-exchanged to produce the same value of high surface stress (with a magnitude of ~1000 MPa) as aluminosilicate glass, although, lithium composition allows to create also a large case-depth (up to 1000 μm). Varshneya *et al.* [33–36] has published a lot on chemically strengthened lithium aluminosilicate glass, which was used as a layer in bullet-proof armor plates. Residual stress profiles in all of these enhanced glasses can be measured with the gradient scattered light method, underscoring the importance of further studies on the subject.

1.4.1 Sequential and single-step preparation method

Double ion-exchange (DIOX) of lithium aluminosilicate (LAS) glass is defined as strengthening by two different species of ions: K^+ and Na^+. Those ions take part in two ion-exchange processes: $K^+ \leftrightarrow Na^+$ and $Na^+ \leftrightarrow Li^+$. The magnitude of surface compression as well as the case-depth needs to be increased to create stronger glass. Our aim was to investigate glasses that fulfill both of those qualities simultaneously. Although $K^+ \leftrightarrow Na^+$ ion exchange process in sodium-containing glasses generates high surface compression up to ~1000 MPa [33],

case-depths remain generally less than 100 µm. Efforts to increase case-depth by increasing the salt bath temperature have resulted in relaxation of the beneficial surface compression. Achieving case-depths greater than 150 µm requires $Na^{+}\leftrightarrow Li^{+}$ ion exchange − the glass sample should contain lithium ions and immersed in molten $NaNO_3$.There are two options to perform this. **(1)** In the **sequential method** of chemical strengthening, the LAS glass containing Li^{+} and Na^{+} ions is immersed in sodium salt bath, followed by immersion in a potassium salt bath, as described by Marusak [37]. **(2)** In contrast, the **single-step method**, introduced by Saunders & Kubichan [38], uses a mixture of salts instead of separate salt baths.

1.4.2 Literature overview of stress profile measurement

Jannotti *et al.* [34] suggested simplifying the measurement procedure by using the so-called direct "fringe-counting" technique, instead of compensator based method for e stress profile measurement in chemically strengthened LAS glass. Jannotti argued that fringe counting is far more reliable method compared to compensator based method, in case of high magnitude of surface compression and steep stress gradients just beneath the surface. Main argument for that was the use of suitable compensator, such as Berek compensator, leads to some level of subjective judgment as whether the (dark) zero-order fringe has been moved to the properly track it down in order to locate the precise position (i.e., sample edge).

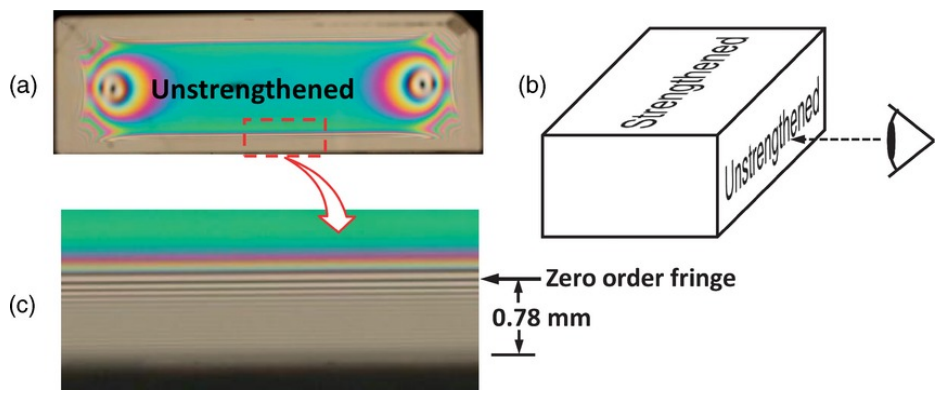

Figure 1.7 (a) Isochromatic fringe patterns as viewed through a polarization microscope of **(b)** unstrengthened surface of the chemically strengthened LAS glass, after Jannotti *et al.* [34]. Also shown is **(c)** an enlarged image of the bottom edge of the unstrengthened face which illustrates the large number of fringes and increasing fringe density toward the edge.

LAS glass slabs were strengthened using Saunders-Kubichan's two-step ion-exchange process. Figure 1.7 shows the isochromatic fringe pattern through polarization microscope of thick specimen (20x10x8 mm). Positions of fringes were measured to determine stress profile. Notice that locating the isoclinic black line (zero stress fringe) enables to determine case-depth value (780 µm), marking the transition from compressive to tensile stress depth-region. Figure 1.8 shows that the isochromatic fringes become indistinct near the surface, mainly as a consequence of the high stress gradient. Figure 1.8 gives much sharper fringes near the surface when viewed under green polarized light with the aid of an optical microscope (10 X objective), with 15 fringes in compression zone and approximately two in the tension zone. These measurements show a maximum compressive stress of 265 MPa. Comparison of Figure 1.9 and Figure 1.10 indicates that is impossible to determine near-surface stresses in case of thick test-specimen.

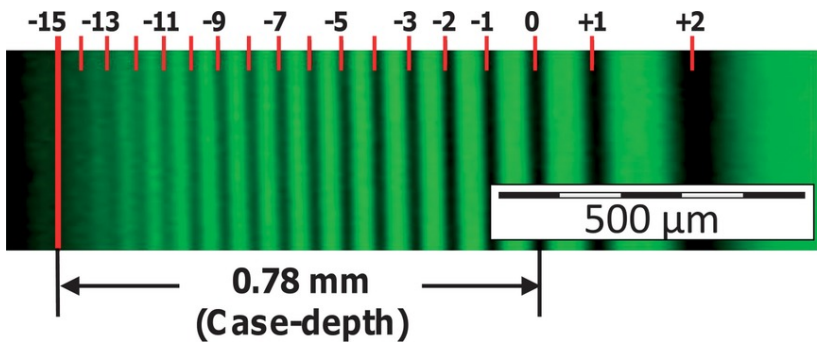

Figure 1.8 Optical micrograph of the isochromatic fringe patterns as viewed through the unstrengthened side using a 10 X objective and a circular polariscope (dark view-field arrangement) with a green optical bandpass filter centered @ 550 nm, after Jannotti *et al.* [34]. A total of 15 fringes in compressive region and two fringes in tensile region are observable.

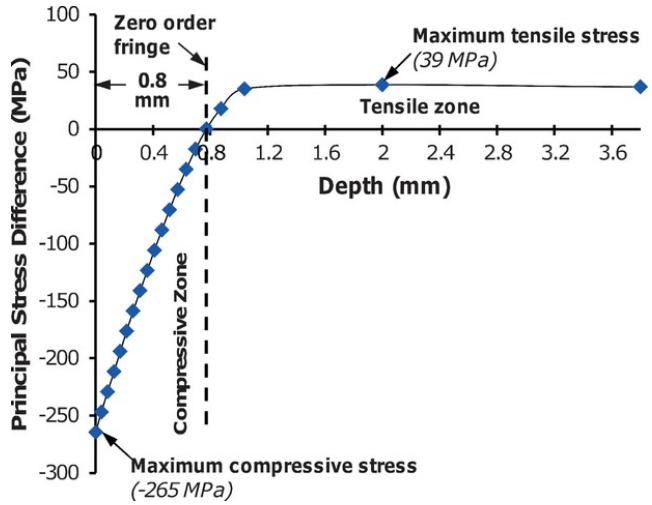

Figure 1.9 Stress profile of a thick (9.9 mm) chemically strengthened LAS glass sample, after Jannotti *et al.* [34].Negative values represent compressive and positive values tensile stresses.

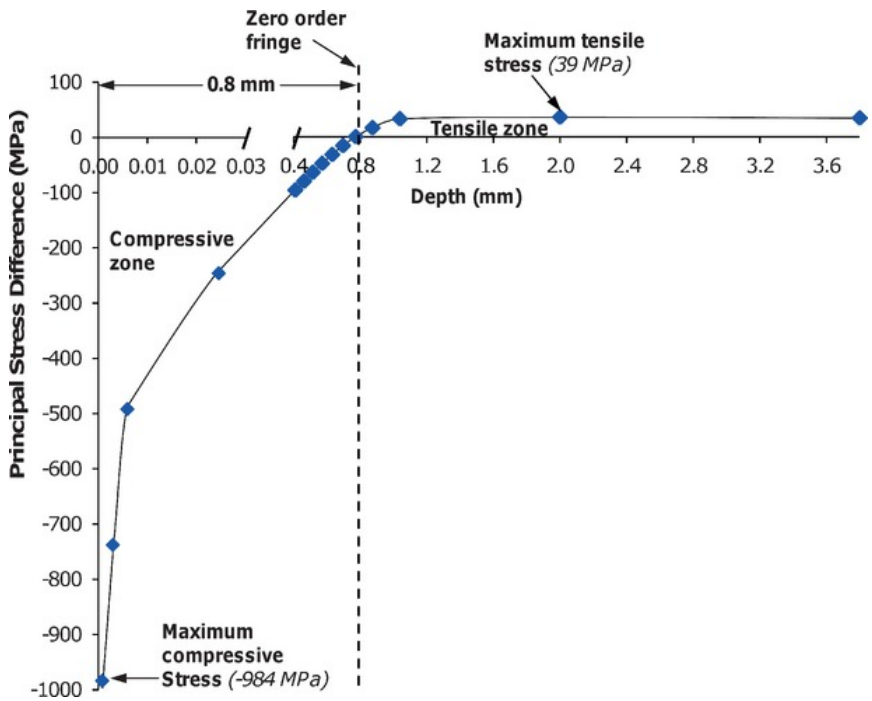

Figure 1.10 Combined stress profiles obtained using the stress profiles the thin (up to 25 μm depth) and the thick specimens, after Jannotti *et al.* [34].

2 OBJECTIVES AND PRIMARY PROPOSITIONS

The main aim of this work was to find new optical methods based on scattered light method to measure stress in chemically strengthened glass.

Within this agenda, the specific objectives of this work were:

- To evaluate stress profile in chemically strengthened glass by confocal detection of Rayleigh scattered laser beam.
- To develop a theoretical model for removing light ray bending influence from stress profiles measured by oblique incidence scattered light method. Such algorithm should be able remove refraction-induced errors from already measured stress profile as a post-processing procedure. Aim was to develop an algorithm that would be suitable to use in automatic polariscope SCALP.
- To investigate stress profiles of chemically strengthened LAS glass.
- To investigate stress inhomogeneity of thermally tempered glass plates using scattered light method.

Primary propositions:

- Confocality enables detection of light from microscopic spatial volume, so it should be possible to use this kind of detection method with scattered light technique.
- Iterative schemes have successfully used in transmitted light photoelasticity to remove the influence of light ray bending from stress results.

This work thus combines theoretical modelling and experimental measurements, as both were needed to reach the objectives.

3 CONFOCAL SCATTERED LIGHT METHOD (PAPER III)

With confocal microscopy, an optical signal can be detected from a microscopic volume in a transparent sample. From a microscopic point of view, a laser beam can be considered as a nearly homogeneous collimated light beam. Confocal microscopy allows scanning within the light beam and collecting Rayleigh scattered light from a microscopic volume. The collected spatial intensity distribution of Rayleigh scattering indirectly characterizes the depth profile of stress in the tempered glass with very high spatial resolution. The diameter of the laser beam is commonly more than 100 μm, while by using high numerical aperture immersion objectives the detected confocal volume can be only a few μm^3. Hence, the confocal imaging of a line along the propagation direction of the laser beam using a micro-translation stage is the same as the observation of a very narrow light beam propagates through the glass plate. The chemically tempered glass sample is at an angle γ (see experimental setup in Figure 3.1) which allows a depth scan into the glass. At each confocal point, the dependence of the intensity of the Rayleigh-scattered light on the polarization state of the incident light can be measured, controlled by the rotation of the wave-plates.

3.1 Principle of the method

3.1.1 The measurement procedure

A uniformly (from both surfaces) chemically strengthened glass plate may be considered as a uniaxial crystal having an optic axis perpendicular to the surface. Secondary principal stresses σ_1 and σ_3 lie in the directions in which the e-ray and o-ray are linearly polarized. If polarized light is incident at an angle to the optic axis of the crystal, it becomes the e-ray which is linearly polarized in the direction of the optical axis, and the o-ray which is polarized in the optical axis, polarized transverse direction.

Similarly to Weißmann & Dürkop [13] we also used the phase modulation optical system consisting of wave-plates to determine the stress profile. Figure 3.1 shows that before entering into a chemically tempered glass plate light from a laser is passed through a rotating λ/2-plate (with rotation angle ϕ) and a fixed λ/4-plate.

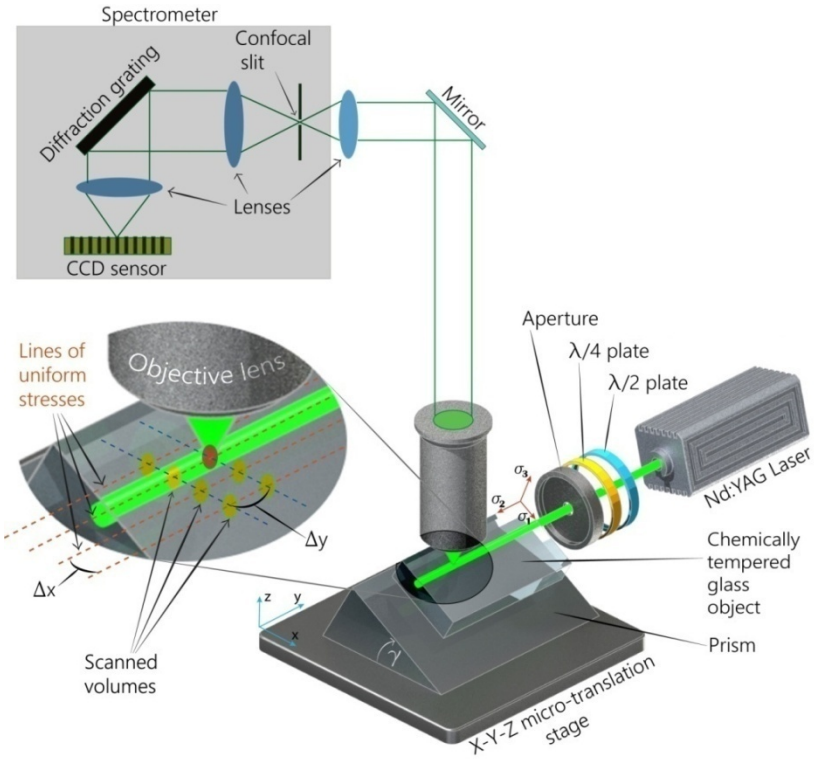

Figure 3.1 The experimental setup for implementing of the phase modulation method for measuring the stress profile. Scattered light outside the confocal point is rejected (cut off by confocal slit). The laser beam is directed along the lines of uniform stress. Full description of experimental setup is given in Paper VI.

For stress measurement the surface of the sample was focused as a reference, and then the confocal point was scanned inside the glass. The λ/2-plate was rotated and at each step the Rayleigh spectrum (see Figure 3.2) of the scattered light was registered. Any kind of compensator (for example a liquid crystal compensator) can be used instead of wave-plate system. The confocal point was shifted by $\Delta y = 100$ μm along laser beam path and the measurement procedure repeated. Note from Figure 3.1, that the depth scan is made perpendicular to the lines of uniform stesses. The depth-scan was accomplished by the motorized movement of micro-translation stage. Slit of the spectrometer enables to create the needed confocality. Voigt function was fitted to measured Rayleigh peak to determine the intensity value of scattered light.

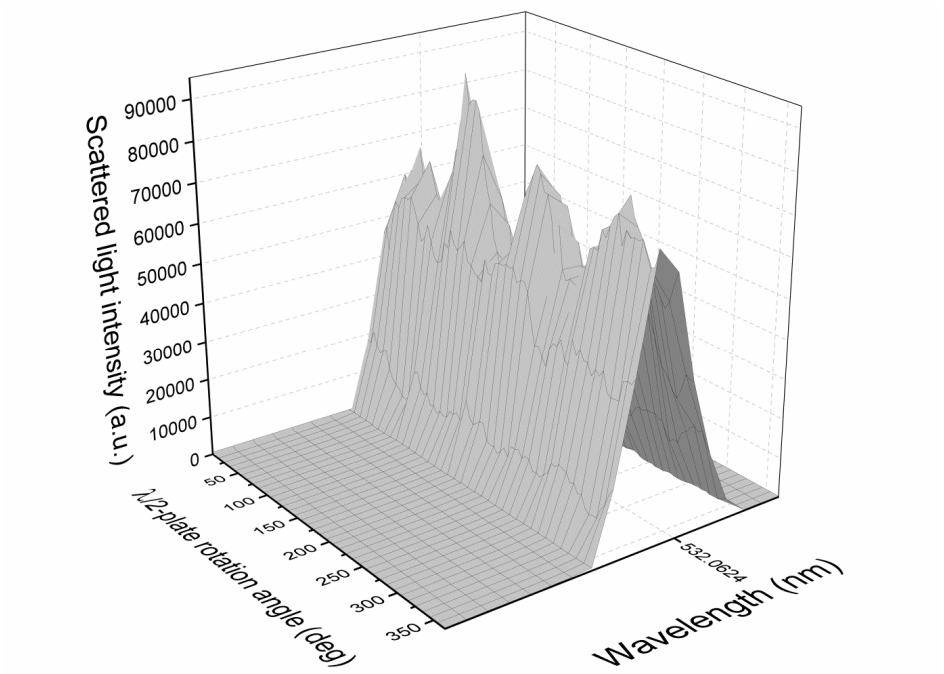

Figure 3.2 Experimental spectra of Rayleigh scattered light from confocal point depending on the rotation angle wave-plate. Rayleigh peak is 0.3nm wide.

It is important to point out here that automatic version of this measurement method should be developed. Other route is to utilize light sheet [39] experimental setups that are already automated for other measurement purposes. Also, oblique incidence version with confocal detection of Rayleigh scattering should be investigated.

3.1.2 Comparison of stress profile and Na^+ ion profile

Figure 3.3 depicts phase difference Δ in chemically strengthened LAS glass. The inset in Figure 3.3 shows two Rayleigh intensity distributions fitted with sinusoids. Using Eq. 1.1 stress profile (Figure 3.4) can be reconstructed from phase difference profile. Near-surface measurements were restricted, although extrapolation gave compressive surface stress of -623 MPa.

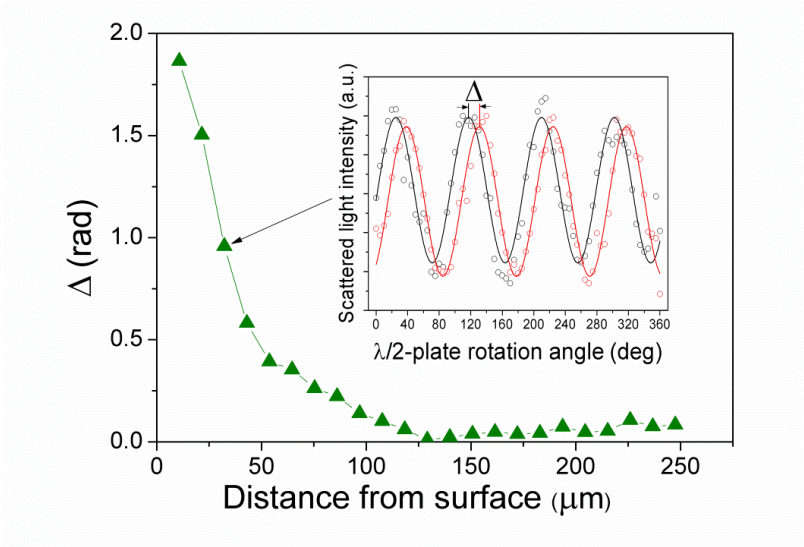

Figure 3.3 Phase difference between two confocally detected points with distance shift of 100 μm.

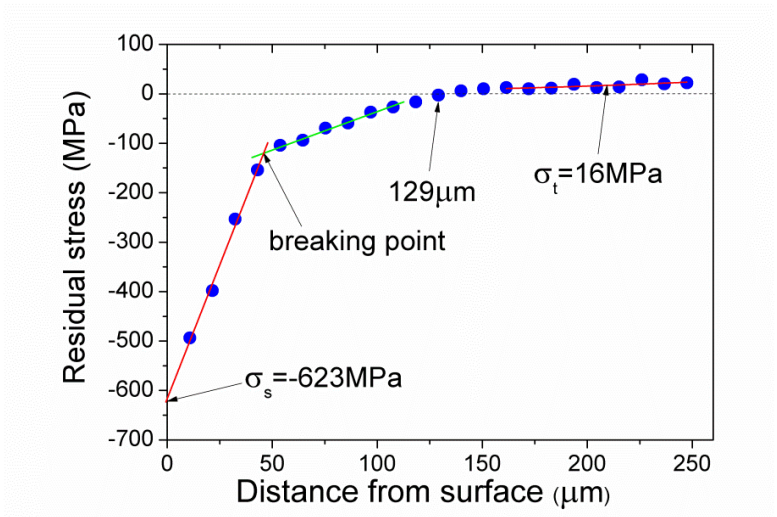

Figure 3.4 The stress profile calculated from phase shift profile from Figure 3.3. The breaking point indicates the crossover between two linear fits for different depth regions.

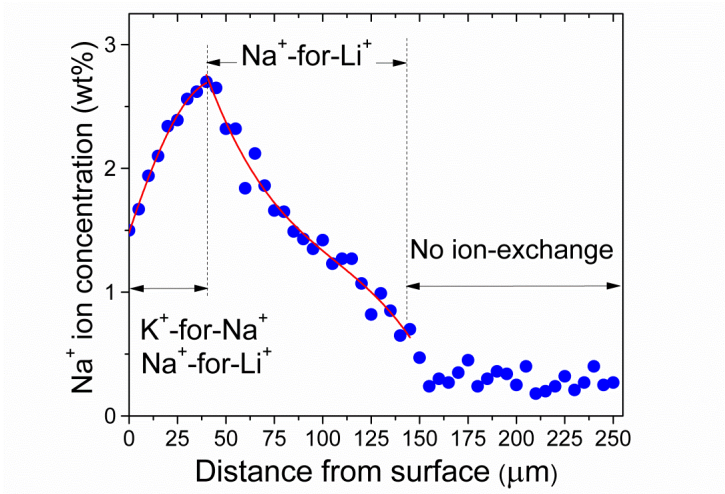

Figure 3.5 Na^+ concentration profile in LAS glass, measured using EDX microanalysis method.

By moving from surface into deeper Na^+ ion concentration initially increases indicating $K^+ \leftrightarrow Na^+$ exchange. At the same time $Na^+ \leftrightarrow Li^+$ exchange also took place, so that Na^+ concentration maximum was established at depth of ~30 μm. Figure 3.5 shows depth-region where only $Na^+ \leftrightarrow Li^+$ occurs. $K^+ \leftrightarrow Na^+$ process creates higher stresses than $Na^+ \leftrightarrow Li^+$.

3.1.3 The dependence of the stress-optic coefficient on the glass composition

The stress-optic coefficient C is influenced by the glass composition, thus making the concentration-stress relation nonlinear. Nissle & Babcock [40] reported that in Na_2O-Al_2O_3-SiO_2-system Na_2O causes stress-optic coefficient to decrease whereas Al_2O_3 to increase. For our samples the Al_2O_3 concentration stayed constant whereas K_2O, Na_2O and Li_2O concentration depth profiles varied. Matusita *et al.* [41] confirmed that Na_2O causes C to decrease and also showed that K_2O causes C to decrease. Smedskjaer *et al.* [42] concluded that alkaline earths ions in aluminosilicate glass have larger impact on C than Al_2O_3. Smedskjaer *et al.* suggested a simple linear regression model to predict the influence of the alkaline earth ions [42].

Available data for LAS glass substrate is $C = 3.3$ Br for LAS and Na^+ ion concentration profile. While increasing Na_2O content simultaneously Li_2O content decreases. During the chemical strengthening process $Na^+ \leftrightarrow Li^+$ equal molar amounts of the ions (or respective oxides) are being exchanged. An important factor is determining which oxide content is most affected by C. The Na^+ ion content profile also indicates the decrease in Li_2O concentration. C

would remain constant if the influence of the composition of Li_2O coincides exactly with Na_2O. According to Matusita *et al.* that's not the case – C is affected by composition as shown in Figure 3.6.

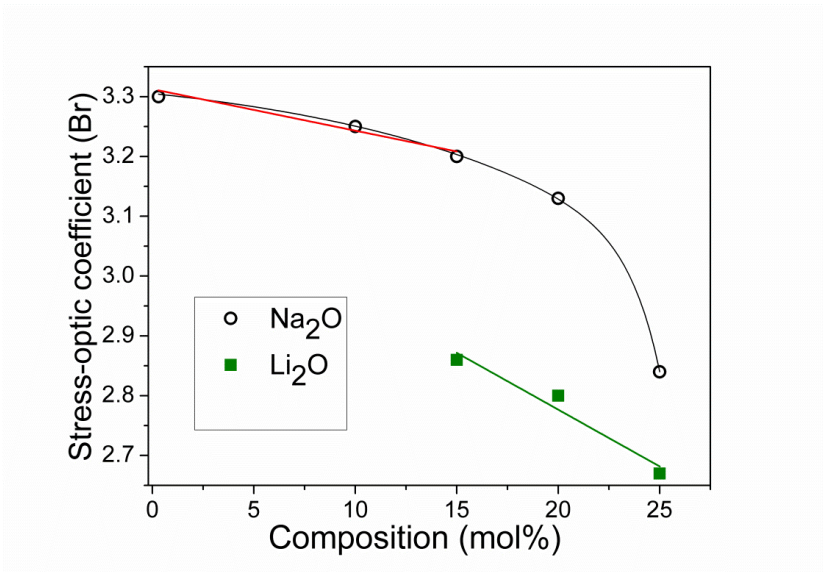

Figure 3.6 Stress-optic coefficient as a function of the composition of aluminosilicate glass Li_2O-Al_2O_3-70mol%SiO_2 according to Matusita *et al.* [41] The compositional influence of system Na_2O-Al_2O_3-70mol%SiO_2 is obtained by combining our own data with the data points of Matusita *et al.* The total dependence is not linear, so we only use of a section that describes C compositional dependency at a lower Na_2O content. The amount of SiO_2 stays constant. (Adapted from Matusita *et al* [41]).

According to simple linear model:

$$C_{predicted}(x) = C_0 + x \cdot \Delta C_{Na2O} - x \cdot \Delta C_{Li2O}\,, \quad (3.1)$$

where C_0 is the intercept, ΔC_{Na2O} and ΔC_{Li2O} are slopes of linear fit from Figure 3.6 and x is the molar change of composition. From Figure 3.7 C_0 = 3.312 Br, ΔC_{Na2O} = -0.058 Br/mol%, ΔC_{Li2O} = -0.019 Br/mol%.

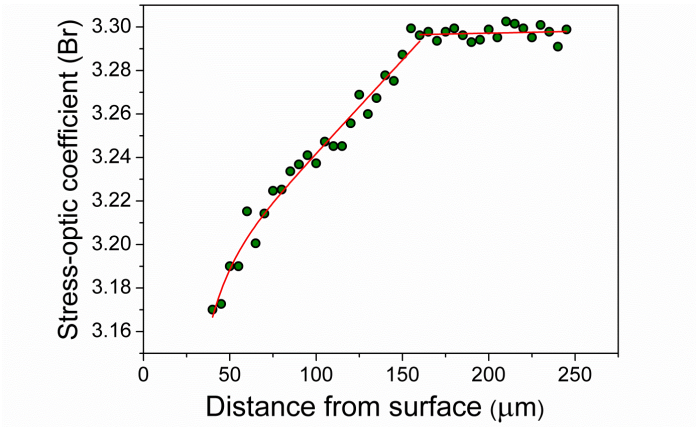

Figure 3.7 Stress-optic coefficient as a function of the distance from the surface. Red line shows two separate fits - a polynomial and a linear.

Figure 3.8 illustrates clear compositional influence. After stress profile is re-calculated using the new values of stress-optic coefficients (from Figure 3.7) then (see Figure 3.8) compositional influence causes the stress increase. At 45 μm depth the compression (that takes compositional influence into account) is 4% higher than the compression value which does not include compositional influence.

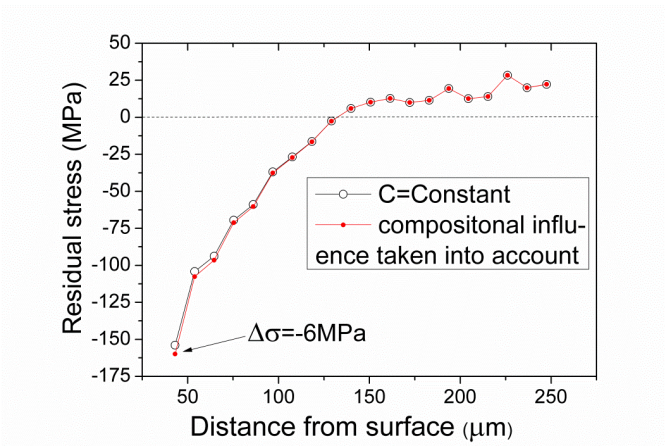

Figure 3.8 Comparison of stress profile calculated on the basis of a constant C and $C(z)$ (red line from Figure 3.7) which takes into account the influence of the composition.

A new micron-scale confocal scattered light method for stress profile measurement in chemically strengthened glass plates was introduced. Compared to alternative stress measurement methods the proposed method has a very high spatial resolution.

4 GRADIENT SCATTERED LIGHT METHOD (PAPERS V AND VI)

4.1 Principle of gradient tomography

The main approach of gradient scattered light method involves ray tracing in the theory of oblique incidence method to remove the influence of light ray bending from stress profiles. The **s**traight **r**ay **i**nversion (SRI) is considered to be the first approximation of the residual stress depth profile. SRI assumes unrealistic scenario that light rays propagate along strictly straight lines. SRI can be used with good precision in case of low stresses (which in turn means low refractive indices). It is used in conjunction with the gradient scattered light theory to determine the first estimate of light ray paths, and a **c**urved **r**ay **i**nversion (CRI) can be performed to obtain (what is hoped to be) an improved approximation to the stress field. CRI simulates realistic situation where light rays actually bend in glass with refractive index gradient. In our case CRI is applied to already measured stress profile hence making it a post-processing algorithm. This approximation is then in turn used to recalculate the ray paths that form the basis for the next iteration until a suitable termination criterion is met. This recursive process which is very similar to Dolovich's scheme (Figure 1.5) is the basis of the gradient scattered light method.

4.2 Experimental evidence of the influence of light ray bending on scattered light fringe patterns (Paper III)

In Paper III setup depicted in Figure 4.1 was used to record Rayleigh scattered light fringe patterns in thermally tempered glass. Such method could be used to measure the precise value of central tensile stresses of thermally tempered glass plate, but not the surface stress values. Reason for that is distorted fringe pattern due to strong light ray bending away from very central region. Note that by moving away from central depth layer (at zero coordinate) towards surface, first fringe pattern gets distorted and then vanishes completely.

The simplified calculation of simulated fringe pattern was done by assuming that light rays propagate along straight path. In realistic situation this is not the case, hence differences between experimental and simulated fringe patterns clearly point out the evidence of light ray bending. Clear indication, that some kind of algorithm should be applied to calculate precise stress profile from experimental fringe pattern shown in Figure 4.2(a).

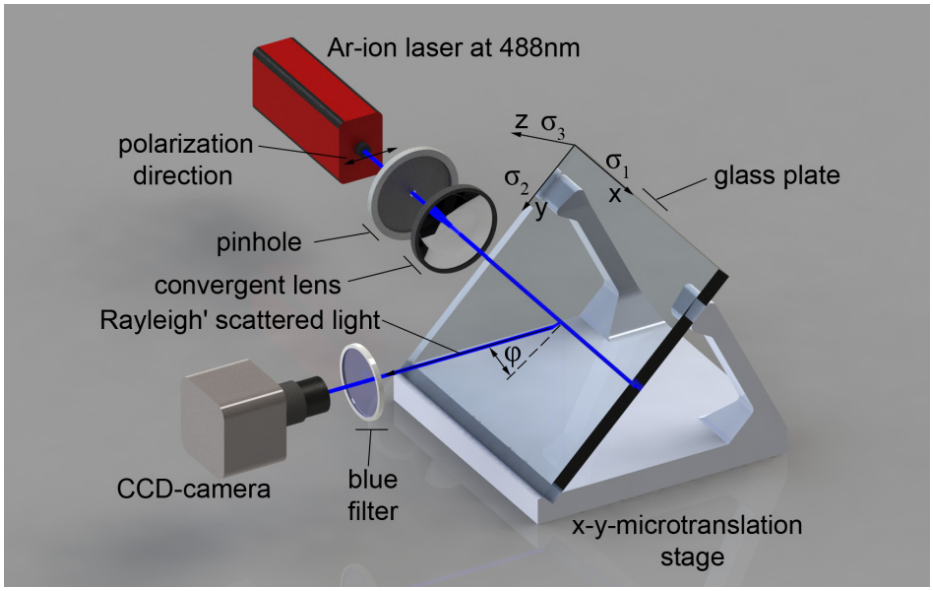

Figure 4.1 Experimental setup. Scattered light is observed perpendicular to propagation direction of laser beam. Observation direction is φ = 45° to plate.

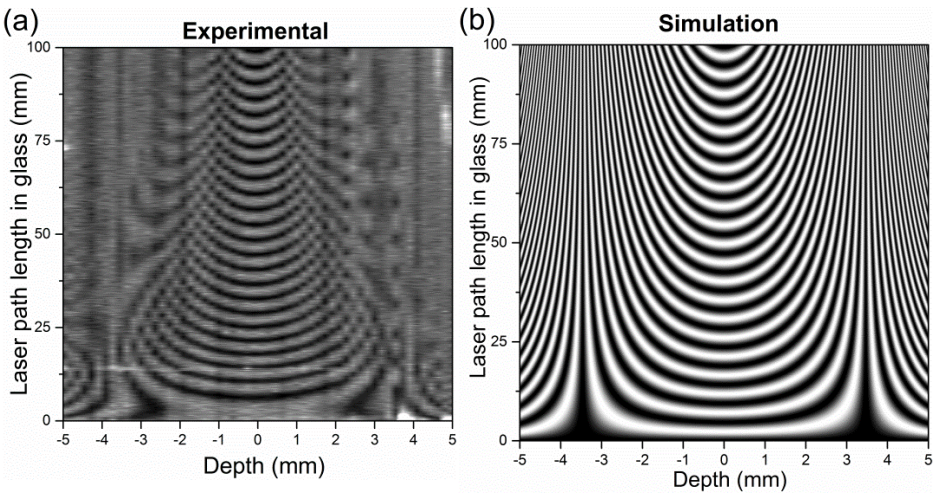

Figure 4.2 (a) Experimental fringe pattern; **(b)** simulated fringe pattern using simplified approach which ignored the light ray bending.

4.3 Oblique incidence scattered light method (Paper V)

In Paper V, the gradient scattered light method was developed specifically for the measurement of micron-scale stress profiles in chemically strengthened glass. **Sca**ttered **l**ight **p**olariscope SCALP-04 (GlasStress Ltd., Estonia) had light beam incidence angle of 45° and was intended for stress measurement in thermally tempered thick glass. To increase resolution new development (SCALP-05) changed the SCALP's angle of incidence of the light beam from 45° to 81.9°. Additionally an iterative approach was developed to remove the influence of light ray bending, which is the direct result of using such a high incidence angle.

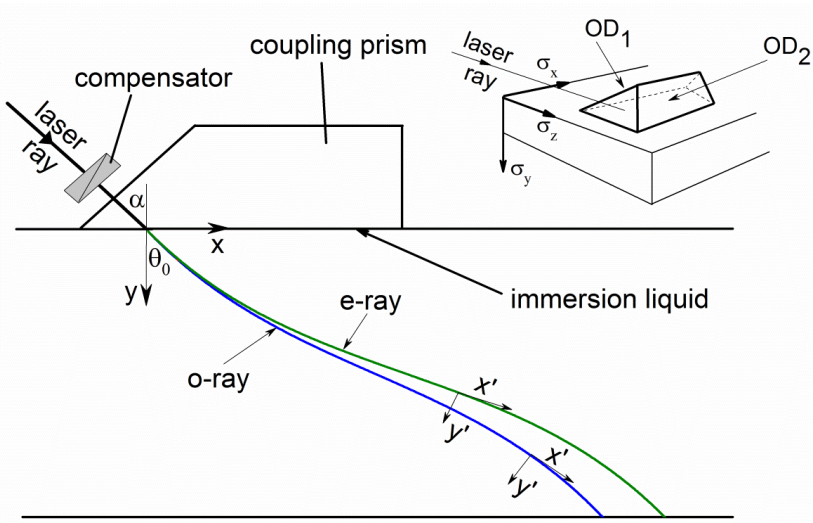

Figure 4.3 The experimental setup for measuring the stress profile. A laser beam is guided obliquely through the strengthened glass plate via a coupling prism. An ultrathin layer of immersion liquid is used between the prism and the glass surface to allow the light to propagate unimpeded. From the observation directions of OD_1 and OD_2, which are at an angle of 45° to the surface of a glass plate to get maximum visibility, the scattered light intensity distribution along the light path could be recorded.

The method is based on Rayleigh scattering, which is excited by an obliquely incident polarized beam through a flat, chemically strengthened (or thermally tempered) glass plate (Figure 4.3). Refractive index fluctuations on length scales, that are small in comparison to the light wavelength, act as dipoles that scatter the light predominantly in the direction perpendicular to the dipole axis. For the theoretical formulation of the method, we assume that the global x-axis is in the plane of incidence and parallel to the top surface of the glass whereas the global y-axis is perpendicular to the top surface of the glass and points into the glass. The global z-axis is chosen to form a left-handed triad with x and y

axes. A local rectangular coordinate system x'-y'-z' is associated with the light beam so that x' is tangent to the ray, y' is on the plane of incidence and z' is perpendicular to the plane of incidence. The clockwise angle between the x' and y axes is θ.

Secondary principal stresses (effective principal stresses) are defined as the stress components which are perpendicular to the propagation direction of the light ray. Those stresses induce Rayleigh scattering fringe pattern that can be observed from both the direction of OD_1 or OD_2. Principal stress σ_y is fixed in the direction of the optic axis and is independent of the propagation direction of the light beam. When the light beam propagates through the glass perpendicular to the z-axis, birefringence is caused by secondary principal stresses σ_z and $\sigma_{y'}$ (see Figure 4.3). The stress field defined in the global coordinate set can be expressed in the local system via the stress transformation equations:

$$\sigma_{x'} = \sigma_x \sin^2\theta + \sigma_y \cos^2\theta \ , \qquad (4.1a)$$

$$\sigma_{y'} = \sigma_x \cos^2\theta + \sigma_y \sin^2\theta , \qquad (4.1b)$$

$$\sigma_{z'} = \sigma_z = \sigma(y), \qquad (4.1c)$$

Within of the glass all tensile and compressive stresses lie parallel to the glass surface and depend only on the depth y: $\sigma_x = \sigma_z = \sigma(y)$. Away from the edges (to avoid the edge stress influence) and in the case of uniform strengthening $\sigma_y = 0$, because glass can swell freely in the direction of the y-axis.

Therefore we can rewrite stresses parallel to surface:

$$\sigma_{x'} = \sigma(y)\sin^2\theta , \qquad (4.2a)$$
$$\sigma_{y'} = \sigma(y)\cos^2\theta , \qquad (4.2b)$$
$$\sigma_{z'} = \sigma_z = \sigma(y). \qquad (4.2c)$$

$\sigma_{x'}$, $\sigma_{y'}$ and $\sigma_{z'}$ (secondary principal stresses) determine the refractive indices for light propagating in the x'-direction by Maxwell's stress-optic relations:

$$n_{y'} - n_u = C_1\sigma_{y'} + C_2(\sigma_{z'} + \sigma_{x'}), \qquad (4.3a)$$
$$n_{z'} - n_u = C_1\sigma_{z'} + C_2(\sigma_{x'} + \sigma_{y'}), \qquad (4.3b)$$

where $n_{y'}$ is the refractive index for the e-ray, $n_{z'}$ is the refractive index for the o-ray and n_u is the refractive index of unstressed glass. Rather than being just a constant, the refractive index n_u may have a depth dependence induced by composition.

The difference ob absolute stress-optic coefficients C_1 and C_2 is the stress-optic coefficient:

$$C = C_1 - C_2. \quad (4.4)$$

$n_{y'}$ and $n_{z'}$ for a known stress profile $\sigma(y)$ are gained by combining Eq. (4.2) and Eq. (4.3):

$$n_{y'} = n_e = n_u + \sigma(y)[C_1 \cos^2\theta + C_2(1 + \sin^2\theta)], (4.5a)$$

$$n_{z'} = n_o = n_u + \sigma(y)[C_1 + C_2]. \quad (4.5b)$$

Wertheim law in integral form combined with Eq. (4.5b) gives the optical retardation along a straight line segment and can be written as

$$\delta(x') = C\int_0^{x'}(\sigma_z - \sigma_{y'})dx' = C\int_0^{x'}(\sigma_z - \sigma_x\cos^2\theta)dx'. \quad (4.6)$$

The incident laser beam induces not only Rayleigh scattering, but also a yellow fluorescence. Consider an incident light beam that is linearly polarized parallel to the observation direction OD_1. The scattered light intensity, consisting of Rayleigh scattering and fluorescence, which can be observed from the directions OD_1 and OD_2, can be written as follows:

$$I_{OD1}(x') = \mathrm{e}^{-\mathrm{k}x'} I_0 \frac{A}{\lambda^4}\sin^2\frac{\delta(x')}{2} + I_\psi \cdot \mathrm{e}^{-\mathrm{k}x'}, (4.7a)$$

$$I_{OD2}(x') = \mathrm{e}^{-\mathrm{k}x'} I_0 \frac{A}{\lambda^4}\cos^2\frac{\delta(x')}{2} + I_\psi \cdot \mathrm{e}^{-\mathrm{k}x'}, (4.7b)$$

where I_0 is the incident light intensity, I_ψ is the intensity of the fluorescence, A is the proportionality factor describing the probability of Rayleigh scattering and signal collection efficiency, λ is laser wavelength and k is extinction coefficient. Fourney & Chang [43] reported that the component I_ψ is considerably larger than the Rayleigh scattered light. To increase the visibility of fringe pattern the component of fluorescence must be removed with an optical filter. The fluorescence is spectrally broad and red-shifted compared to the incident wavelength. For example, if the exciting light is blue, the fluorescence is usually yellow.

4.4 Measurement of optical retardation distribution

To resolve stresses near the surface, optical retardation was measured using SCALP-05. An ultra-narrow (diameter ~50 µm) laser beam with a wavelength of 635 nm was passed through the glass surface at an incidence angle of 81.9°

(Figure 4.3). A glass prism was used to couple light into the surface layer of the glass. The optical retardation distribution was calculated from the fringe pattern of Rayleigh-scattered light using optical phase modulation method. The polarization state of the laser beam was periodically modulated using a liquid crystal compensator. This means, in turn, that the scattered light intensity along the laser beam (as recorded by the camera) should also be modulated in correlation to the compensator. But only the Rayleigh scattered light intensity follows such kind of modulation, while any parasitic light does not. Therefore the synchronization of those modulations can act as a quality indicator showing the percent of camera pixels along the image of the beam path where the optical modulation during the measurement was good enough to be accepted for stress calculation. The measured retardation distribution was always too rough for direct stress calculation and hence must be smoothed by fitting with polynomials (see Figure 5 in Paper V). Near the points where the laser beam enters the glass panel and where it hits the other surface of the panel, a parasitic light scattering occurs and speckle pattern may be visible.

Prior to measuring, a window cleaning liquid was sprayed on the sample and the surface was wiped clean with an optical cloth. An ultra-thin layer of Cargille immersion oil was used between the prism and the glass surface to allow unimpeded propagation of light. Measurement of the stress profile was conducted away from edges at the central area of the glass plate surface to avoid the influence of edge stresses. Three repeated measurements were performed and the mean value was calculated.

4.5 Optical retardation along curved ray path

Optical retardation along curved ray path $\delta_c(y)$ corresponds to experimental optical retardation $\delta_{exp}(y)$. Realistic situation is simulated if light ray bending is calculated from known stress profile $\sigma(y)$.

A glass plate can be considered consisting of thin planar layers (Figure 4.4), with the light beam propagating along straight line within each layer. Therefore, the optical retardation distribution through each layer can be written as:

$$\delta_0(y) = \frac{C \sin^2 \theta_0}{\cos \theta_0} \int_0^y \sigma(y) dy \quad (4.8a)$$

$$\delta_1(y) = \frac{C \sin^2 \theta_1}{\cos \theta_1} \int_0^y \sigma(y+y_2) dy \quad (4.8b)$$

$$\dots\dots\dots\dots\dots\dots$$

$$\delta_i(y) = \frac{C \sin^2 \theta_i}{\cos \theta_i} \int_0^y \sigma(y+y_i) dy \quad (4.8c)$$

Integral is starting from zero for each layer, so Eq. (4.8) does not provide a smooth distribution of optical retardation. Optical retardation $\delta_i'(y)$, which

takes into account the accumulating optical retardation in all previous layers, is written as

$$\delta_i'(y) = \delta_i(y - y_i) + \delta_{i-1}'(y_i), \qquad (4.9)$$

where $\delta_{i-1}'(y_i)$ is calculated in a similar manner based on layer $i-2$, etc.

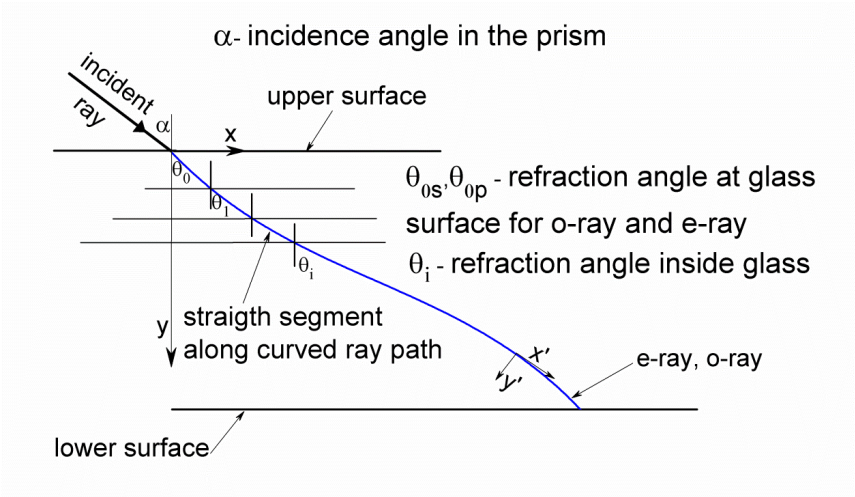

Figure 4.4 Light ray passing through a flat glass plate divided into thin layers.

A set of *if*-conditions refines smooth optical retardation distribution along the curved ray path:

$$\delta_c(y) = \begin{cases} \delta_0(y), \ y_0 < y < y_1 \\ \delta_1(y - y_1) + \delta_0(y), \ y_1 < y < y_2 \\ \cdots\cdots\cdots\cdots\cdots \\ \delta_i(y - y_i) + \delta_{i-1}'(y), \ y_i < y < y_{i+1} \end{cases} \qquad (4.10)$$

4.6 An iterative approach to remove the influence of light ray bending from scattered light tomography (Papers V and VI)

In Papers V and VI we describe an iterative scheme to remove the influence of light ray bending from measured stress profile. In case of extremely deep DOL values (200-1000 μm) it was necessary to introduce new version this of iterative scheme that is more adapted for experimental data analysis.

Curved ray inversion for stress profile calculation can be written as follows:

$$\sigma_{CRI}(y) = \begin{cases} \dfrac{\cos\theta_0}{C\sin^2\theta_0}\dfrac{d}{dy}\delta_c(y), & y_0 < y < y_1 \\ \dfrac{\cos\theta_1}{C\sin^2\theta_1}\dfrac{d}{dy}\delta_c(y), & y_1 < y < y_2 \\ \cdots\cdots\cdots\cdots\cdots\cdots & \\ \dfrac{\cos\theta_i}{C\sin^2\theta_i}\dfrac{d}{dy}\delta_c(y), & y_i < y < y_{i+1} \end{cases} \quad (4.11)$$

In the Rayleigh-scattered light tomography, optical retardation data can be interpreted assuming that the probing light rays are straight lines within the strengthened glass under study. SRI is extremely useful if the refractive bending of light rays is small but can result in significant reconstruction errors in case of large incidence angles (such as the 81.9° incidence angle in SCALP-05). SRI yields accurate results for low incidence angles, such as 45° (used in SCALP-04). Therefore the case-depth along with the mid-plane stresses of glass plate were very accurately determined by using SCALP-04 where the laser beam passes through the glass plate at 45° angle.

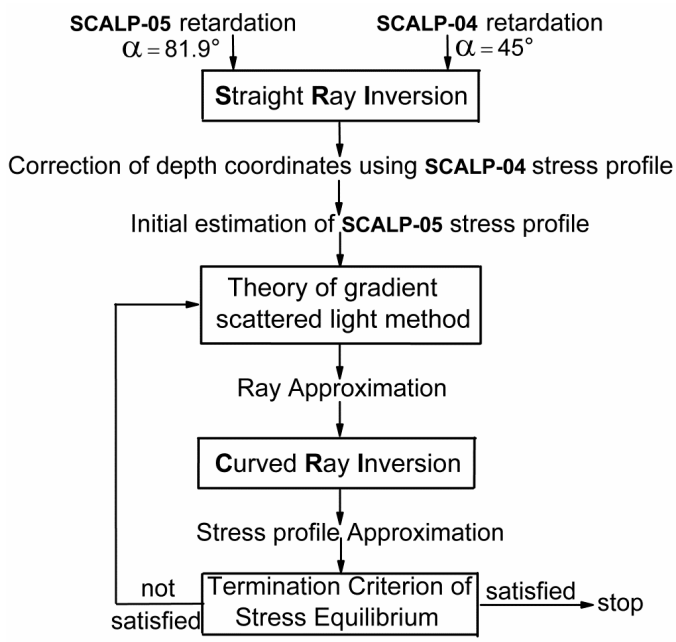

Figure 4.5 An iterative scheme of **CRID**: curved-ray inversion is combined with depth coordinate correction for more accurate stress profile calculation from the optical retardation data.SCALP-04 measurement is needed for depth coordinate correction for glass plates that have: **(1)** thickness >1.3 mm (because laser beam exit point is not observable); **(2)**DOL > 350 μm.

The sequence of iterative steps (Figure 4.5) was used to correct depth coordinates and to remove the influence of light ray bending in scattered light tomography:

(1) Straight ray inversion (45°).First, the optical retardation $\delta_{04}(x')$is measured by using SCALP-04 and the stress is obtained as:

$$\sigma_{SRI}(x') = \frac{1}{C\sin^2\alpha}\frac{d}{d\eta}\delta_{04}(x')$$

(2) Straight ray inversion (81.9°).The optical retardation $\delta_{05}(x')$ is measured by using SCALP-05and from that an initial estimate of the stress profile is calculated by same equation as in previous step.
(3) Correction of depth coordinates. Correct DOL which is not affected by ray bending is obtained from the SCALP-04 stress profile. Hence this DOL is used to correct depth coordinates of the SCALP-05 stress profiles.
(4) Ray approximation. The curved trajectories of the e-ray and the o-ray are calculated by using the previously obtained $\sigma_{SRI}(y)$ in the ray equation.
(5) First iteration of CRI+DOL-correction (CRID).The stress profile is recalculated from $\delta_{05}(x')$ using an algorithm where the curved trajectory of the rays is taken into account**.**
(6) Calculating stress equilibrium is used to test the validity of the stress profiles.

Notice here the similarities between our and Dolovich's scheme (Figure 1.5). Dolovich used this scheme for transmitted light photoelasticity. The *strain-gradient theory* is much more complicated compared to our *theory of gradient scattered light method* because many rays are needed to probe the glass sample under study.

4.7 Testing the iterative algorithm to remove refraction-induced errors in case of compressive or tensile surface stresses (Paper VI)

In Paper V we did testing of iterative scheme only in case of profiles with compressive surface stresses. It was shown that if light ray propagates along curved ray path (see Figure 4.6) then experimentally measured optical retardation is blue dashed line in Figure 4.7(a).

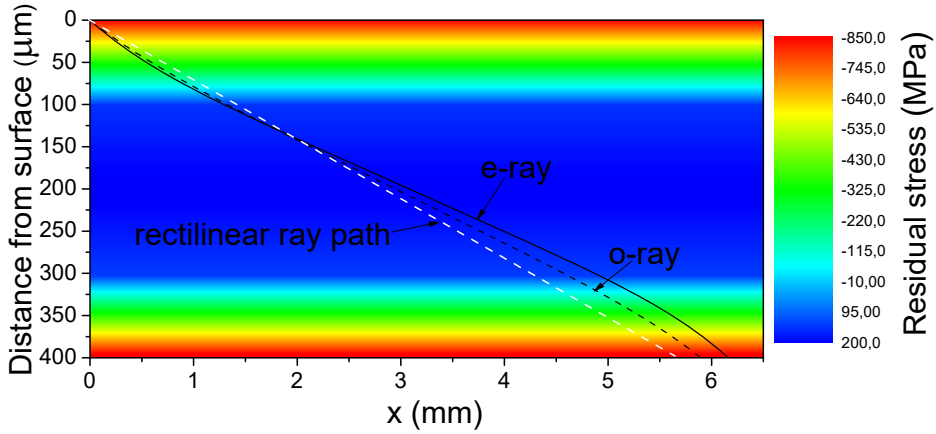

Figure 4.6 Curved ray paths of light propagating through stress field of chemically strengthened glass plate. Note, that the y-axis is magnified by a factor of approximately 16 compared to the x-axis.

Figure 4.7(b) illustrates how iterative scheme removed the influence of light ray bending with only few iterative steps (see inset of Figure 4.7(b)) Notice, from Figure 4.7(b) that SRI first gives a stress estimate, that is erroneous compared to reference stress profile. Although if curved light ray paths are calculated from refractive index profiles which in turn calculated form $\sigma_{SRI}(y)$ then the next iterates are rapidly closer to known stress profile.

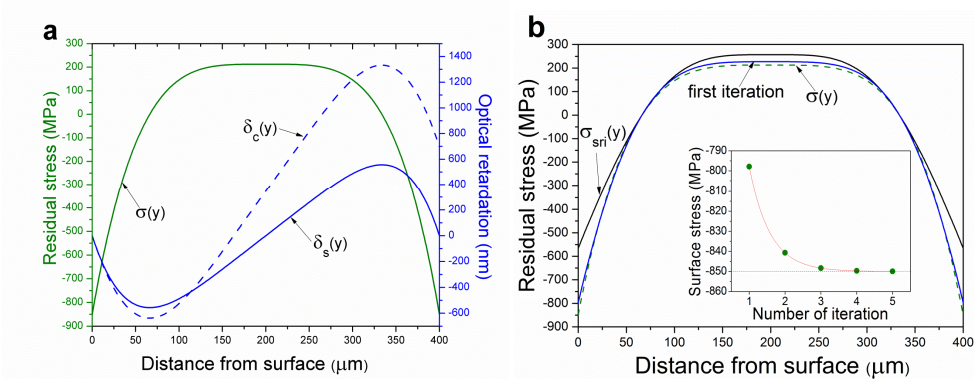

Figure 4.7 (a) Initially known stress profile $\sigma(y)$ (green line), optical retardation along curved ray $\delta_c(y)$ (dashed blue line), optical retardation along rectilinear ray path $\delta_s(y)$ (blue line). **(b)** Initially known stress profile $\sigma(y)$(dashed green line), straight ray inversion $\sigma_{SRI}(y)$ (black line), first iteration (blue line). The inset shows surface stress value as a function of CRI iteration number.

In Paper VI we took under investigation profiles with simulated tensile surface stresses. In fact, it is possible that stress profile exhibits an unusual behavior where the outermost layers of the surface are in tension, rather than compression. Tensile stresses can be induced into glass surface by chemical ion-exchange process in which small ions from external source are exchanged for larger ions in the glass surface (the inverse of the normal chemical strengthening method). Note that such inverse process makes glass actually weaker. This kind of ion-exchange was first reported by Stewart & Young [44], and later by Ernsberger [45] as a method for revealing the surface flaws of glass.

Figure 4.8 compares the reconstructed stress dependence of iteration number. For compressive stress the maximum reconstruction error was reduced from 15% (using SRI, 0^{th} iteration) to 2% (using 1^{st} iteration of CRI). For tensile stress the maximum error was reduced from 26% (SRI) to 9% (using 1^{st} iteration of CRI). Figure 4.9 show that compressive surface stresses converge $k_c/k_t = 1.7$ times faster than tensile surface stresses.

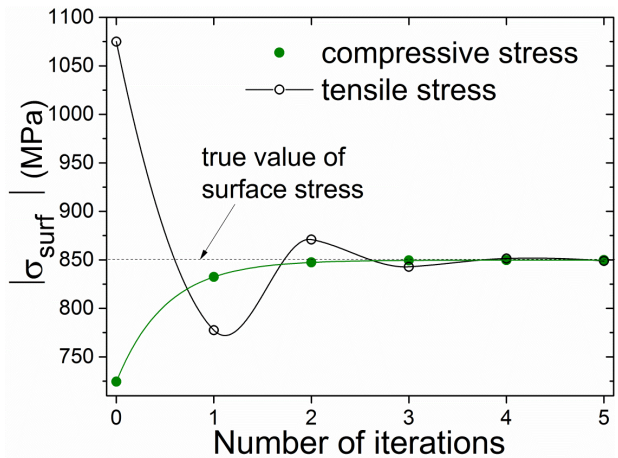

Figure 4.8 Absolute value of surface stresses as a function of iteration number.

Figure 4.8 also illustrates that compressive and tensile surface stresses converge differently: compressive stresses converge monotonically whereas tensile stresses oscillate about the real value. Such different behaviour can be explained as follows. In case of tensile stresses, SRI (0^{th} iteration) results a surface tension value of 1075 MPa. This value is used to calculate the first estimation of surface refractive index. The increase of tensile stress causes the decrease of refractive index (Figure 4.10(a)), hence near-surface light ray propagation angles θ_i are corrected towards higher values ($\theta_i > \alpha$). 1^{st} iteration of CRI leads to surface stress that is calculated using higher θ_i values. CRI gives a new tensile stress value of 775 MPa. This in turn results in higher refractive indices and lower values of light propagation angles. 2^{nd} iteration yields a surface tension of

870 MPa, which once again leads towards higher values of θ_i than in previous iteration. So the reconstructed tensile stresses oscillate about the real value.

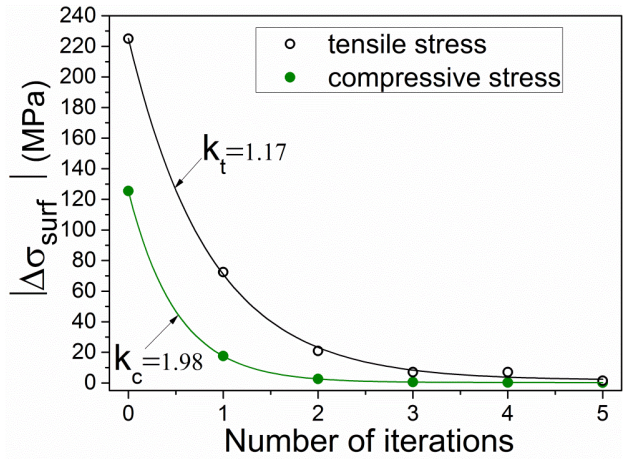

Figure 4.9. Stress-induced errors of tensile and compressive stresses as a function of the iteration number. The absolute values of error due to light ray bending nearly exponentially approach 0 with increasing iteration number. Hence the dependence was fitted with $|\Delta\sigma| = Ae^{-kx}$, where k indicates the speed of convergence.

In contrast, an increasing surface compression (by absolute value) causes the increase of refractive index (Figure 4.10(b)). Those stresses converge monotonically because iterative approach corrects the refraction angle only towards lower values.

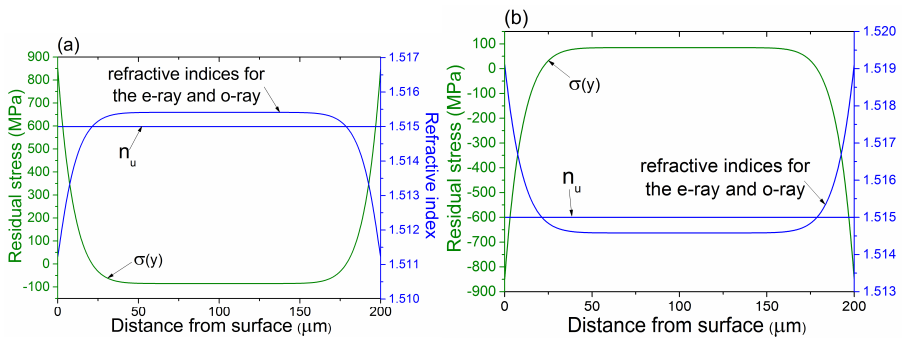

Figure 4.10 (a) The depth profiles of tensile stress and corresponding refractive index; **(b)** The depth profiles of compressive stress and corresponding refractive index. Note that actually refractive index profiles are different for the e-ray and o-ray, but they are too close spatially to be separated from this graph.

5 BUILD-UP OF STRESS OF CHEMICALLY STRENGTHENED LITHIUM ALUMINOSILICATE GLASS (PAPER V)

This section is extension of Paper V. Here we tested **SRID** and **CRID** algorithms on experimental data. Papers V and VI illustrated that CRI worked well in simulations. Here we wanted to find out whether it also reduces the influence of light ray bending.

5.1 Samples and characterization methods

LAS glass plates with dimensions 40x20x3 mm^3 were chemically strengthened in a molten salt mixture consisting of 80 mol% KNO_3 and 20 mol% $NaNO_3$.To study the temperature dependence of the stress profile, the glass plate was strengthened for 24 hours at 440, 460, 480 or 500°C. To investigate the stress build-up, the substrate glass plate was immersed into the mixed molten salt at a temperature of 480°C either for 1, 4, 8, 16 or 24 hours. The purities of both KNO_3 (Otsuka Chemical Co., Ltd.) and $NaNO_3$ (Kanto Chemical Co., Ltd.) were >99%.The stress-optic coefficient was $C = 3.3$ Brewster ($10^{-6}MPa^{-1}$).The detailed description of determination of C is given in Paper V. The glass composition in Table 1 was determined experimentally using EDX microanalysis.

TABLE 1 Composition of the LAS glass sample derived from EDX microanalysis.

	SiO_2	Al_2O_3	Li_2O	MgO	Na_2O	K_2O	TiO_2	ZrO_2
Mol%	69.9	13	9.8	1.2	0.4	0.2	1.8	3.7
Wt%	64.5	20.5	4.5	0.7	0.349	0.3	2.2	7

By lapping away glass from one edge of the sample we could prepare a surface that exposed the changing Na^+ ion concentration distribution and a depth scan could be carried out. Na^+ concentration profile was determined with energy-dispersive X-ray (EDX) microanalysis by using Helios NanoLab 600 electron-ion dual beam microscope equipped with 50 mm^2 X-Max SDD-detector (Oxford Instruments).To avoid charging effects, the sample was coated with a thin Pt film. The elemental depth profiles were determined point-by-point across the sample's cross-sectional area near the sample surface with a step size of 5 μm. The measurement of Li^+ ion concentration is methodically impossible using EDX microanalysis.

Surface refractive index of some samples was measured by using the ellipsometer GES-5.

5.2 Shift of case-depth

First, it is important to establish whether the diffusion depth is generally deeper than DOL or vice versa. According to Garfinkel & King [46] ($Na^+ \leftrightarrow Li^+$ ion-exchange), the normalized stresses calculated directly from Na^+ ion concentration give ~20 % deeper stress profile compared to the measured one. Also in the case of $K^+ \leftrightarrow Na^+$ ion exchange, the diffusion depth of K^+ was reported to be also ~20 % deeper than DOL [47]. Figure 5.1 indicates that our results fulfill the criteria of Na^+ diffusion depth being deeper than the layer of compressive stresses.

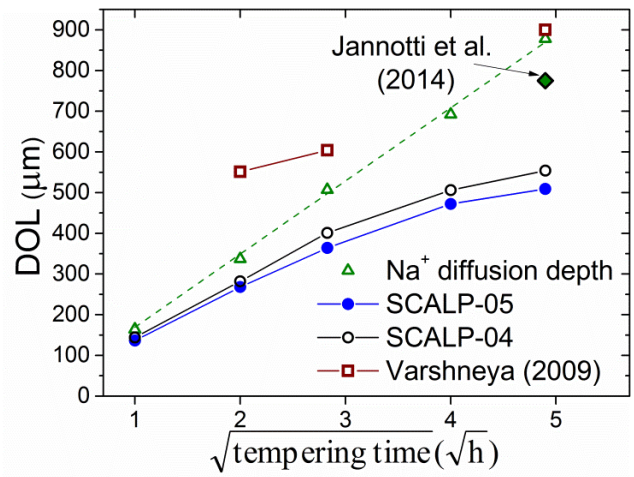

Figure 5.1 Dependence of experimental Na^+ diffusion depth and the DOL on the square root of the diffusion time. The dashed green line represents the calculated diffusion depth of Na^+ ions by $2\sqrt{D_{IE}t}$, where the diffusion coefficient $D_{IE} = 1.8 \cdot 10^{-8}\text{cm}^2/\text{s}$ was calculated directly from experimental diffusion profile of sample that was strengthened for 1h. All samples were ion-exchanged in molten salt bath at 480°C.

Figure 5.1 shows a comparison between DOL from our measurement (SCALP-04 and SCALP-05), Varshneya's [33] DOL values and Na^+ diffusion depths. Varshneya's DOL values for samples strengthened for 4 h and 8 h were deeper than the SCALP-04 DOL values. Figure 5.1 also shows that Varshneya's DOL values are deeper than diffusion depth. Yet, Jannotti's DOL of 24 h strengthened samples is smaller and Varshneya's DOL is approximately equal to diffusion depth. Possible reasons for those differences might be diffusion "blocking". Sglavo [48] showed that the "blocking" effect can also be caused due to contaminated salt bath by the presence of Ca and Mg in the KNO_3 bath (also in amounts of few tens of ppm).

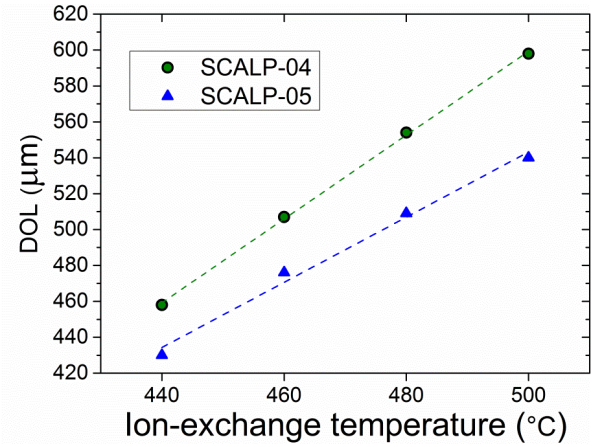

Figure 5.2 Dependence of the DOL and Na^+ diffusion depth on the exchange bath temperature. All samples were ion-exchanged for 24h.

Figure 5.2 shows that DOL values measured with SCALP-04 were in deeper than the ones measured with SCALP-05. This phenomenon is a clear sign that DOL shift occurs due to a combination of incidence angle difference in polariscope and higher increasing refractive indices due to higher exchange temperature. Higher incidence angle leads to a more rapid increase of ΔDOL, because the bending effect is strongest when the light propagates perpendicularly to the refractive index gradient vector.

Figure 5.3 explains the origin of refraction-induced DOL shift (ΔDOL), which is defined as difference between assumed and actual DOL values. The light ray, incident on the glass plate at 81.9°, is assumed to propagate along a straight path. Due to light ray bending both the e-ray and o-ray actually propagate along curved path and the actual DOL value is deeper than the assumed DOL value. The same explanation can be attributed to DOL shift observable from Figure 5.1, where the stresses measured at 45° angle show higher DOL values. Figure 5.3 also demonstrates that the exit point of the light beam cannot be used as an indicator of the magnitude of light ray bending. The e-ray and o-ray beams can coincidentally exit the plate at the same point as the assumed straight ray path. Another problem is that the initially narrow laser beam (with a diameter of 50 µm) is widening strongly along the path. An indicator of such widening is a larger stray light dot at the exiting point of the glass plate.

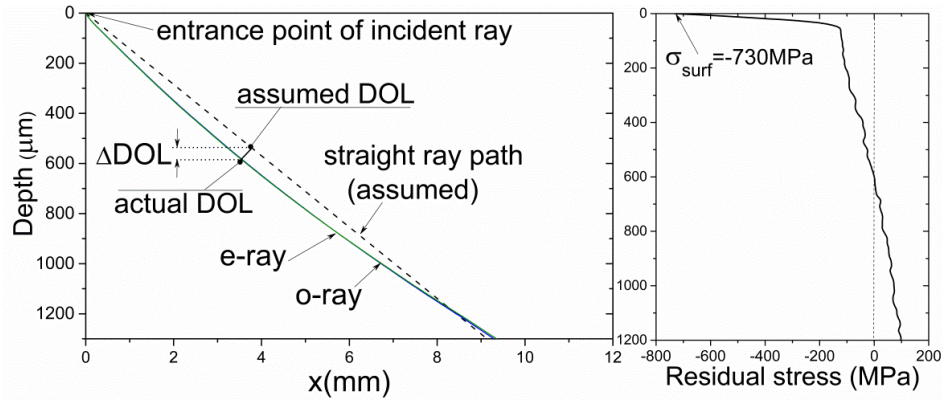

Figure 5.3 Curved paths of ordinary and extraordinary ray propagating through the stress field of a LAS glass plate chemically strengthened at 500°C for 24 h. The true ray paths of the e-ray and o-ray are compared to apparent straight ray path. The corresponding residual stress profile is shown on the right panel. Note that the scale of the lateral position is magnified by a factor of approximately 9 compared to the depth.

The main reason for DOL shift is a strong influence of glass composition on the light ray paths. Hence, to further investigate DOL shift we compare experimental and calculated ΔDOL values. ΔDOL were calculated as follows: Surface refractive index of the glass plate strengthened for 24 h at 500°C was measured with ellipsometer. Ellipsometric measurement gives the sum of unstrengthened substrate refractive-index n_{sub} and surface refractive-index change:

$$n_{ellipso} = n_{sub} + \Delta n. \quad (5.1)$$

Δn consists of stress-induced component Δn_{stress} and compositional component $\Delta n_{composition}$:

$$\Delta n = \Delta n_{stress} + \Delta n_{composition}. \quad (5.2)$$

Refractive index depth profile of the e-ray and o-ray can be written as:

$$n_e(y) = n_u + \sigma(y)[C_1 \cos^2\theta + C_2(1 + \sin^2\theta)], (5.3a)$$
$$n_o(y) = n_u + \sigma(y)[C_1 + C_2], (5.3b)$$

where n_u is unstressed (compositional) refractive index, $\sigma(y)$ is stress profile (measured with SCALP), parameters C_1 and C_2 are the absolute stress-optic coefficients of the material for the considered wavelength and θ is the propagation angle in glass. Notice that Eq. 5.3a and Eq. 5.3b incorporate both compositional component n_u and stress induced components $\sigma(y)[C_1 \cos^2\theta + C_2(1 + \sin^2\theta)]$ and $\sigma(y)[C_1 + C_2]$ for the e-ray and o-ray, respectively. The

difference of $C_1$and C_2gives the stress-optic coefficient: $C = C_1 - C_2$. The change of stress-induced refractive-index at the surface can be written as

$$\Delta n_{stress} = \frac{n_{o.surf} + n_{e.surf}}{2} - \Delta n_{sub}, \quad (5.4)$$

where $n_{o.surf}$ and $n_{e.surf}$ are respectively surface refractive indices of the ordinary ray and extraordinary ray.

The final step is to convert the measured stress profile $\sigma(y)$ and Δn to a compositionally induced refractive-index profile $n_u(y)$. The exchanged ions locally affect the refractive-index by three physical mechanisms: ionic size, ionic polarizability and photoelastic effect due to induced stress. While the latter mechanism has been found to dominate the index exchange for $K^+ \leftrightarrow Na^+$ ion-exchanged glass [49], it is small in comparison to the other two effects in $Ag^+ \leftrightarrow Na^+$ exchanged glass [50]. In practice, one does not need to know the ionic polarizability. Instead, an empirical value of maximum index change Δn is correlated to the normalized stress profile. Hence the unstressed refractive-index profile is obtained as:

$$n_u(z) = n_{sub} + \Delta n \frac{\sigma(y)}{\sigma_{surf}}. \quad (5.5)$$

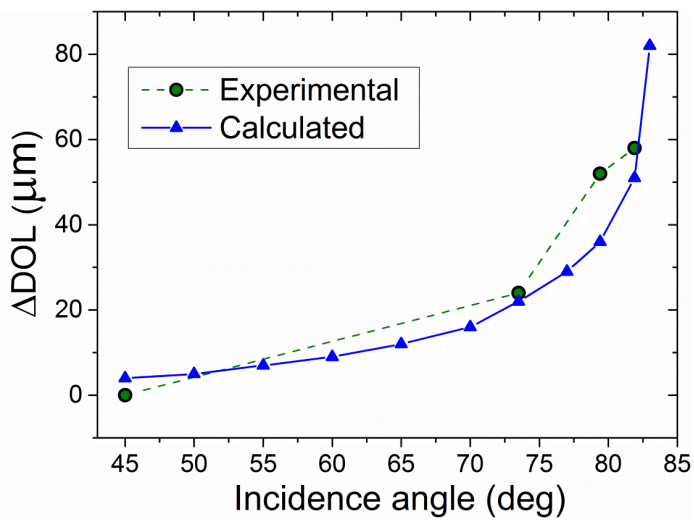

Figure 5.4 Dependence of the DOL shift on the incidence angle α. The samples were ion-exchanged for 24h at 500°C.Experimental DOL values were obtained by changing the incidence angle of the light beam in SCALP-05 polariscope to various values 73.5°, 79.4°or 81.9°. SCALP-04 was used for 45° angle measurement. The calculated ΔDOL values were obtained by combining ellipsometry and stress data for ray tracing (see Figure 5.3).

Figure 5.4 shows a comparison between the experimental and calculated ΔDOL values. In the case of higher incidence angle, ΔDOL increases more rapidly, because the bending effect is strongest when light propagates perpendicularly to the refractive index gradient vector. In contrast, if the light ray propagates at 45° incidence angle, both experimental and calculated ΔDOL value is significantly smaller compared to α=81.9°. In practical situations, it is much more convenient to measure experimental DOL shift value (by using case-depth data measured with 45°-angle polariscope SCALP-04), than to use ellipsometric data in combination with ray tracing to gain calculated DOL shift values from the deflections of light rays.

5.3 Equilibrium of stresses

Compressive and tensile stresses are balanced through the thickness of a tempered glass plate ($\int_0^h \sigma dz = 0$). Due to a combination of experimental errors and errors introduced by reconstruction algorithms, perfect stress equilibrium does not occur. Papers V and VI showed that in the case of numerical simulations we were able to determine the percentage of errors due to the influence of light ray bending. Once we are dealing with experimental stress profiles, such an option is no longer available, because the exact stress profile is unknown. Equilibrium of the stresses is hence the only indicator to test whether the measured stress results can be trusted. Equilibrium error is defined as the difference between compressive and tensile stress areas under the stress profile.

In the previous section we showed that the shift of DOL is dependent on specific incidence angle used in polariscope. Therefore we analyze different options to incorporate this new data into the reconstruction scheme. Table 2 compares stress equilibrium of SRI and the two new versions of reconstruction algorithms that both incorporate DOL correction as an additional post processing method. Simplest of the two is **SRI** in combination with **D**OL correction (those two forms a new algorithm called **SRID**): the stress is calculated from the optical retardation using SRI and then the depth coordinate is corrected by taking DOL value from the SCALP-04 measurement. An iterative scheme in Figure 4.5 describes the second new algorithm, **CRI** combined with **D**OL correction (**CRID**): in this algorithm the depth coordinates are first corrected the same way and then CRI algorithm is applied.

TABLE 2 Summary of stress equilibrium results for different reconstruction algorithms. $\int \sigma^+ dz$ is the area under the tensile zone.

Sample	Time (h)	Tempe-rature (°C)	SRI $(\frac{\int_0^h \sigma dz}{\int \sigma^+ dz})$	SRID $(\frac{\int_0^h \sigma dz}{\int \sigma^+ dz})$	CRID $(\frac{\int_0^h \sigma dz}{\int \sigma^+ dz})$
A	1	480	-2.3%	0.8%	–
B	4	480	13.5%	11.5%	3.4%
C	8	480	12.7%	4.8%	0.1%
D	16	480	12.8%	6.9%	2.4%
E	24	480	16%	8.2%	3.4%
F	24	440	20.6%	12.6%	8.7%
G	24	460	17%	8.7%	3.8%
H	24	500	21%	2.7%	-1.8%

Table 2 indicates that by applying the DOL correction, in average two times better stress equilibrium is achieved. The DOL correction in combination with CRI generally also yields a better stress equilibrium (about five times better, compared to SRI). In accordance with the data presented in Table 2, we have established that the termination criterion (Figure 4.5) of the iterative scheme should be the lowest percentage of equilibrium error. SRI and CRI should both be considered for best option.

5.4 Stress build-up

Figure 5.5 shows a comparison between our results and the stress profile of similarly strengthened LAS glass by Jannotti *et al.* [34]. Note that sample preparation and substrate glass composition were very similar, except our sample was strengthened at 5°C higher temperature. Compared to Jannotti's stress profile, our stress profile has lower surface compression, deeper breaking point and shallower DOL value. Note from Figure 5.5 that Jannotti's stress profile has a shallower depth of the breaking point and simultaneously a deeper DOL. These changes are mutually correlated, granting the desired stress equilibrium. This indicates that if either the near-surface stresses or the DOL value is erroneously measured, the equilibrium of stresses is no more a good indicator. Figure 5.5 also illustrates that the Na^+ concentration profile peak (at depth of 100 µm) is deeper than the breaking point.

Figure 5.6 shows that just after the breaking point the stresses remain almost unchanged for samples strengthened for 4h and 8h (change is only 2 MPa) in the depth-region ranging from 82 µm to 108 µm. The sample that was strengthened for 1 h did not exhibit such behavior. Varshneya and Jannotti were unable to resolve the precise shape of the stress profile near the breaking point. However, such phenomenon was also observed by Inaba *et al.* [51] while using

a transmitted light photoelastic stress measurement (based on conventional optical microscope with retardation imaging system).

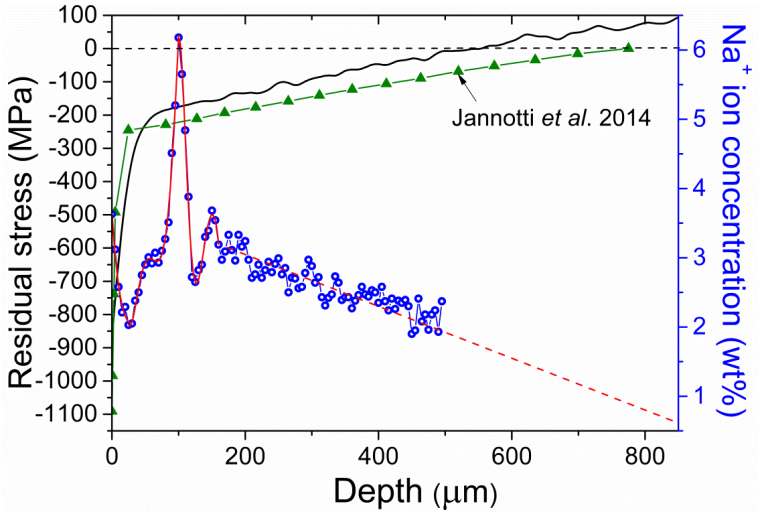

Figure 5.5 The stress profile and Na^+ ion concentration profile in chemically strengthened LAS glass (ion-exchanged for 24 h at 480°C). Jannotti's glass (Ion-Armor™) **[34]** is strengthened for 24 h in salt bath mixture consisting of 80 mol% KNO_3 and 20 mol% $NaNO_3$ at temperature 475°C. DOL values for our measurement and Jannotti's are respectively 554 μm and 775 μm. Jannotti measured surface stress of 1091 MPa, while our result was 877 MPa.

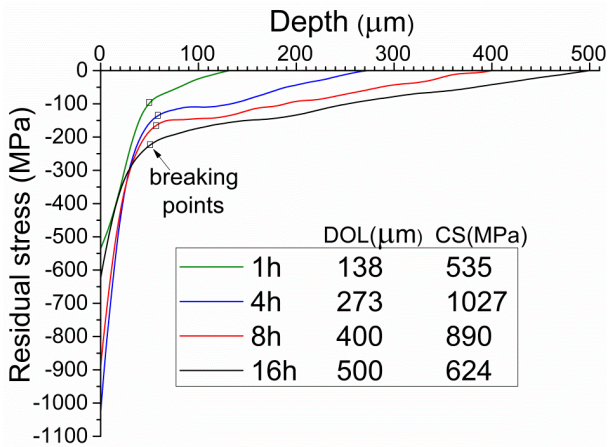

Figure 5.6 Comparative plot of the residual stress profiles in unbroken plates of LAS glass as a function of ion-exchange treatment time. All samples were ion-exchanged at 480°C. CS represents a value of the compressive surface stress.

Figure 5.7 shows constant stresses in the depth-region after the knee-shaped breaking point, where the stresses remain almost unchanged. Note, that this depth-region of constant stresses is most dominant for the sample strengthened for 24 h at 500°C. Figure 5.7 also shows similar tendency for samples strengthened for 440°C, 460°C and 580°C although by a smaller extent. This can be attributed to the relaxation of stresses, because the sample strengthened for 1 h did not exhibit such behavior. Those constant stresses are equivalent to breaking point itself shifting deeper, because the same stress value remains constant in depth. In conclusion, in the sample strengthened for 24 h at 500°C, the compressive stresses are effectively shifted 4 times deeper, due to the depth-region of constant stresses after the breaking point.

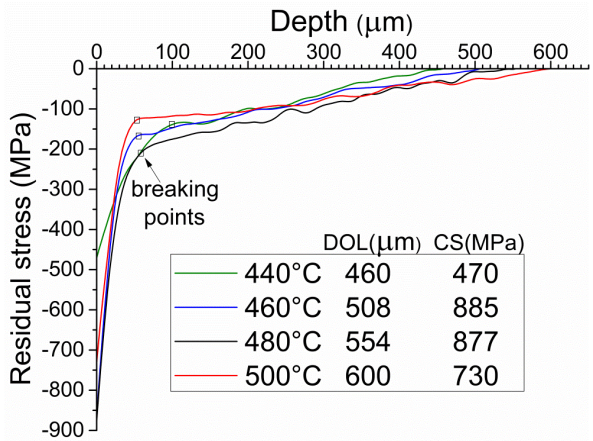

Figure 5.7 Comparative plot of the residual stress profiles in unbroken plates of LAS glass as a function of ion-exchange salt bath temperature. All samples are ion-exchanged for 24h.

5.5 Surface stresses compared to modulus of rupture (MOR)

The fundamental principle of ion-exchange strengthening is the replacement of Na^+ ions with physically larger K^+ ions from the molten salt surrounding glass. The physical pressure thus altered at the surface adds a substantially higher tensile stress requirement to the external forces required to grow cracks. Similarly, the resistance to abrasions is also increased. Effectively, glass is much stronger.

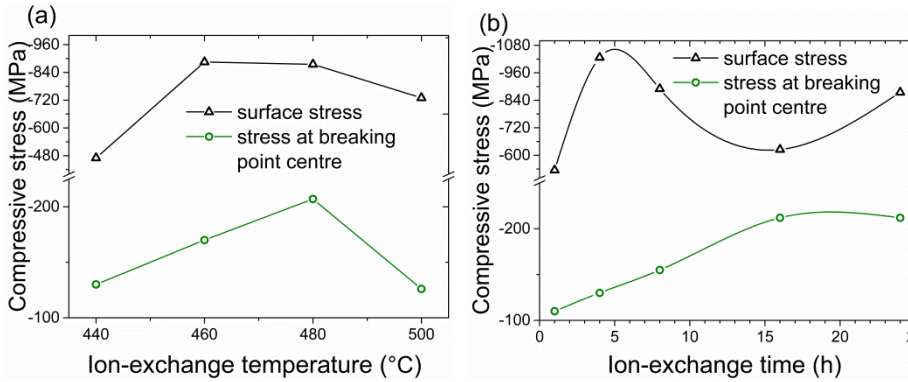

Figure 5.8 (a) The dependence of the compressive surface stress and stress at the knee-shaped breaking point centre on the tempering time duration. 480°C is more beneficial because breaking point stress is the highest if one has to choose between 460°C and 480°C. **(b)** The dependence of the compressive surface stress and stress at the centre of knee-shaped breaking point on the tempering time duration.

Figure 5.8 (a) indicates that maximum value for surface stress is produced if exchange temperature is 460–480°C. Notice that stress value at breaking point centre is maximum at 480°C, which means that overall strength of glass is probably highest at 480°C. Figure 5.8 (b) illustrates some of the issues with surface stress. As a function of ion-exchange treatment time, the average surface stress of glass increases rapidly, peaks (at 4 h), and then actually declines in the longer period. Typical MOR's dependence on strengthening time follows the same tendency [52]. Chemical strengthening often exhibits such stress-relaxation effects, whereby the greatest compressive stress value of a surface later decreases. Although, notice that surface stress value for 24 h strengthened sample has once more risen close to the level of plateau.

Samples from brittle materials can be examined through Weibull plots derived from MOR's of a representative population of samples and testing in a manner analogous to the actual product use. The Weibull plot approximates the cumulative distribution function of failure probability for a particular sample under varying loads. Thus, it is possible to estimate the stress corresponding to a given failure rate of interest. Figure 5.9 shows Weibull modulus plots of the strengths of the LAS glass. The $NaNO_3$ content has been varied form 0 mol% to 30 mol% (0 wt% to 26.5 wt%) and compared with data obtained with unstrengthened and unstrengthened-plus-abraded specimens. The plot suggests superiority of 20mol% $NaNO_3$ salt mixture over others.

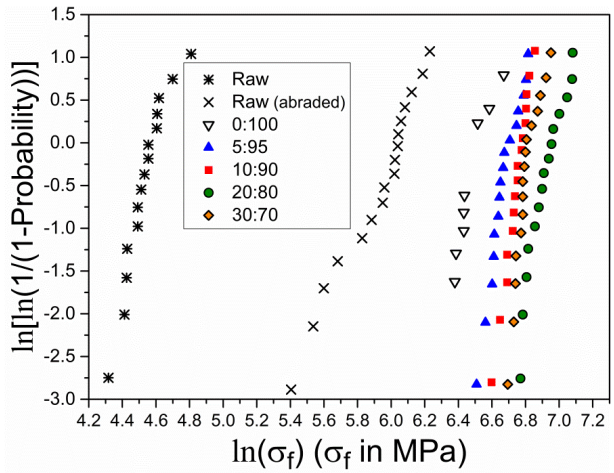

Figure 5.9 Weibull modulus plots of MOR (ring-on-ring method [53]) for LAS glass as a function of ion exchange at 475°C for 24h in varying ratios of $NaNO_3/KNO_3$ mixed salt baths (Adapted from Varshneya and Spinelli **[33]**).

Figure 5.10 shows a plot of the MOR versus $NaNO_3$ concentration in the salt mixture from 0 percent to 30 percent $NaNO_3$, suggesting superior results in the 20:80 bath. One sample from this plot [33] is comparable to our measurement results. It is the one strengthened for 24 h in 20:80 molar ratio of $NaNO_3/KNO_3$ mixed salt bath at 475°C. Our sample is strengthened at same conditions, except temperature was 480°C. For this sample MOR value is 1000 MPa and our surface stress value was 877°MPa. This means that unstrengthened glass strength is about 90°MPa which is in realistic value (for tempered glass plates unstrengthened strength was reported to be ~60°MPa [Paper I]).

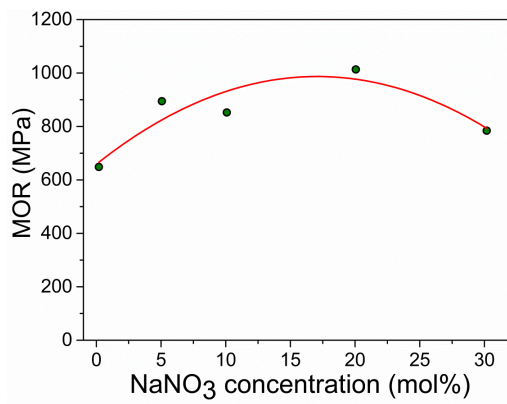

Figure 5.10 The Plot of MOR values (@ 50% breaking probability, from previous graph) versus $NaNO_3$ concentration in the $NaNO_3$+KNO_3 salt baths (calculated from Figure 5.9). Data points are fitted with parabola (red line).

5.6 Stress equilibrium as a function of known surface stress and light incidence angle

The aim of this section is to investigate the influence of surface stress and incidence angle to equilibrium errors - the latter being an important indicator of the correctness of our measurements and calculations. In simulation we used self-equilibrating stress depth profile: $\sigma(z) = \sigma_{surf} \cdot d^{-m} \frac{m+1}{m} \left[|(d-z)^m| - \frac{d^m}{m+1} \right]$, where d is half-thickness of glass plate and m is polynomial order. This polynomial was formulated by Brodland & Dolovich [54] to produce symmetric, self-equilibrating stress distributions, like those that typically arise in a uniformly strengthened (from both sides) glass plate. By increasing m the shape of the simulated stress profile becomes more characteristic to chemically strengthened glass. In this simulation d = 1.5 mm, m = 5 and $n_{prism} = 1.515$. To calculate ray paths of the e-ray and o-ray the absolute stress-optic coefficients were taken to be $C_1 = -7.77 \cdot 10^{-7}$ MPa^{-1} and $C_2 = -4.077 \cdot 10^{-6}$ MPa^{-1} [54], which yields to stress-optic coefficient of C = 2.573 Br.

Let us point out that these simulations analyze only the stress component of reconstruction errors due to light ray bending. In realistic situation of course, ion-exchange process changes the composition of surface and hence also the compositional refractive indices. Compositional influences affect the precise determination of depth coordinate Therefore new reconstruction algorithm CRID incorporates depth coordinate correction by taking DOL value from an additional SCALP measurement with smaller incidence angle (such as 45°). It would be very hard to construct a reliable purely theoretical model that can predict compositional influences. CRID algorithm is used to reconstruct experimental stresses, and CRI algorithm to calculate stresses from simulated optical retardation. In both cases depth coordinate shift is either removed (for CRID) or totally absent (for CRI). Hence stress results calculated by these two algorithms are comparable. In similar logic SRID (for experimental data) and SRI (for simulations) are comparable. Table 2 shows that average SRID equilibrium error of experimental stress profiles is 7 %. For comparison Figure 5.11 shows that the same value at for SRI simulations (at average experimental surface stress value of 755 MPa and at incidence angle of 81.9°) is 11%.

45° incidence angle is sufficient to measure stress in thermally tempered glass plate. However, to achieve a spatial resolution high enough to measure the stress profile in chemically strengthened glass, a narrow laser beam is passed through the surface layer of the glass at a considerably larger incidence angle of 81.9°. This way, the increased length of laser beam path becomes observable and increase in resolution is achieved. Also in case of higher incidence angle, a more rapid increase of refraction-induced equilibrium errors can be seen from Figures 5.11 and 5.12(a), because the bending effect is strongest when light propagates perpendicularly to the refractive index gradient vector. The 81.9° is close to incidence angle for which the e-ray and the o-ray are not yet spatially

separated and the maximum length of light beam path is observed. This angle is not fixed because it depends on, among other parameters such as absolute stress-optic coefficients, mostly on the magnitude of stresses.

By further increasing the incidence angle, desirably increasing the resolution, spatial separation of the e-ray and o-ray occurs, and the observable scattered light fringe pattern disappears, so that the optical retardation can't be measured. The spatial separation of those beams is greater at grater depths, which means that experimental measurement of optical retardation has a depth limit (in case of 81.9° this depth limit is 1.3 mm).

Figure 5.11 shows a comparison of refraction induced equilibrium error of SRI percentage dependence of surface stress for specific incidence angles of SCALP. Error of equilibrium is very sensitive to changes in incidence angle: changing the angle from 81.9° to 79.4° (3 % change) results in rapid 40 % decrease of equilibrium error. Hence by increasing the incidence angle we gain in resolution but lose in higher equilibrium errors.

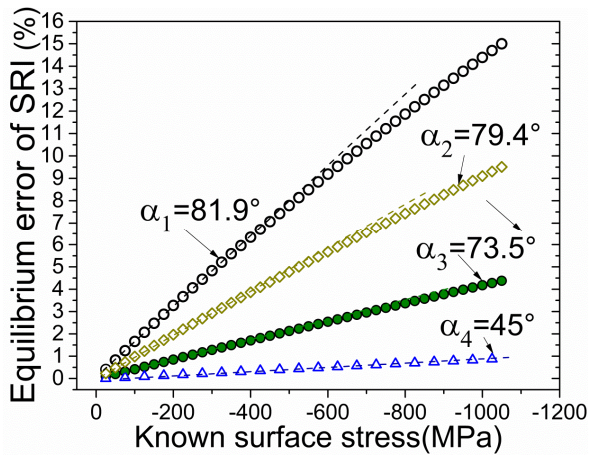

Figure 5.11 Correlation between known surface stress and equilibrium error**.** The actual experimental incidence angles of SCALP were used in simulation. Equilibrium error is defined as: $100\% \cdot (\int_0^h \sigma_{SRI} dz \,/\, \int \sigma_{SRI}^{+} dz)$, where $\int_0^h \sigma_{SRI} dz$ is difference in the areas of compressive and tensile zones and $\int \sigma_{SRI}^{+} dz$ is the area of tensile stress zone.

Important question here is whether SRI or CRI algorithms produce stress reconstruction errors, that are smaller than experimental errors. From Paper V the precision of SCALP-05 is ±3.7 % for stresses > 20 MPa. Figure 12(a) illustrates that maximum value of SRI equilibrium error is 15 % and the corresponding surface stress reconstruction error of SRI is18 %. If maximum value of CRI equilibrium error (see Figure 5.12(b)) is 1.2 % then the corresponding surface stress reconstruction error of CRI is 2.9 %. Therefore, SRI does not and CRI does produce smaller reconstruction error than experimental errors.

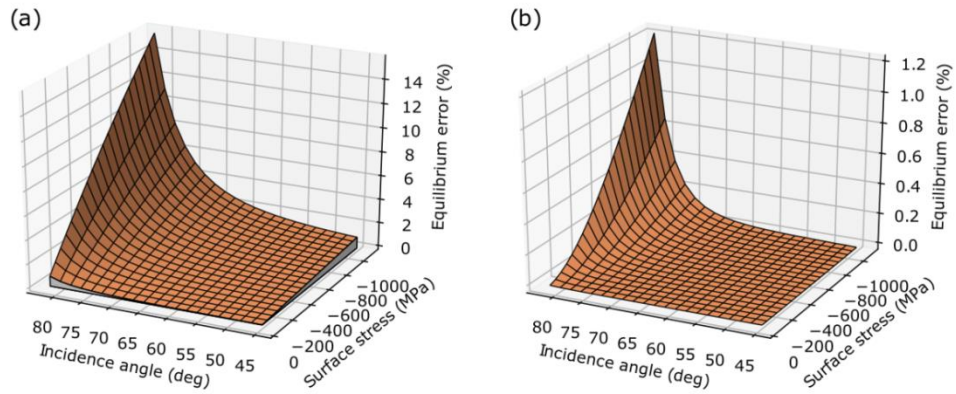

Figure 5.12 (a) SRI equilibrium error; **(b)** first iteration of **CRI**'s equilibrium error.

Figure 5.12 shows a comparison between equilibrium error percentages of SRI and CRI as a function of both surface stress and incidence angle. It illustrates a more general insight into the effectiveness of CRI in removing the refraction induced equilibrium errors. Figure 5.12 (a) shows that incidence angle 82° and surfaces stress 1050 MPa result in maximum equilibrium error of SRI. For this particular simulation maximum SRI's equilibrium error 15% (Figure 5.12 (a)) is reduced to 1.2% (Figure 5.12 (b)) if CRI algorithm is applied. These graphs would enable us to choose the optimum incidence angle for measurement of sample with a particular surface stress. Although CRI is so effective that even for extreme cases it reduces the equilibrium error to less than experimental error.

6 STRESS IN THERMALLY TEMPERED GLASS PLATES

6.1 Correlation between surface stress and bending strength (Paper I)

In accordance with the European Standard prEN 12150-2:2004 to determine if a product meets to the definition of thermally tempered soda lime silicate safety glass, the initial type testing shall include the following: **a)** mechanical strength according to EN 12150-1 (also EN 1288-3:2000) or **b)** fragmentation test according to EN 12150-1:2000. Subsection 5.2.2.4 "Measurement of surface pre-stress" of the same standard sounds: "The manufacturer may also use surface pre-stress measurement as a means of product control. If this is done, then all test specimens shall be measured prior to testing. This will show the relationship between surface pre-stress and mechanical strength fragmentation."

Therefore, European standards require the use of the 4-point bending test and/or the fragmentation test. Both tests are destructive, time-consuming and expensive.

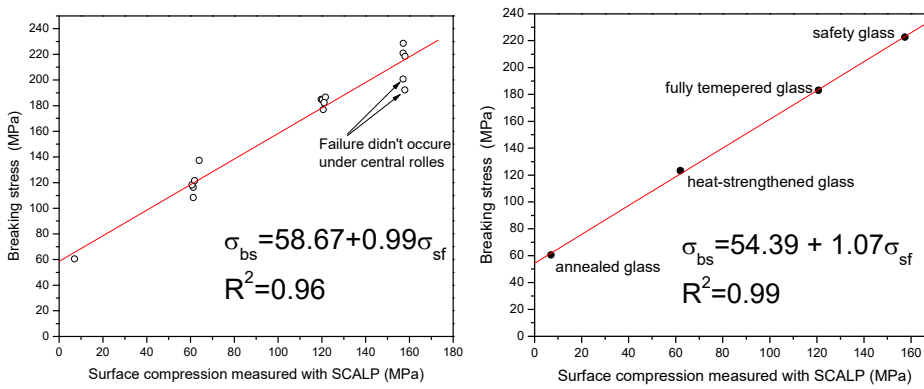

(a) (b)

Figure 6.1 Bending strength (breaking stress) vs glass surface compression measured with SCALP-04: **(a)** all data points, **(b)** averaged for each kind of thermal treatment. Two measurement points where failure didn't occur under central rollers were excluded.

Our goal was to investigate correlation between surface compression measured with SCALP and standardized 4-point bending test. In this test, SCALP-04 was used with an angle of incidence of 45°. In a somewhat simplified form, the relationship between the bending strength σ_{bs} and surface stress σ_{sf} can be expressed as follows:

$$\sigma_{\mathrm{bs}} = \sigma_0 + k\sigma_{\mathrm{sf}}, \quad (6.1)$$

where σ_0 is a value close to the strength of the annealed float glass σ_a and k is an empirical coefficient ($k \cong 1$). Since σ_a is known, the measurement of surface residual stress determines the flexural strength of the glass. Figure 6.1 shows linear relationship between the residual stress and flexural strength of glass panels, which confirms the results of other authors. It may be reasonable to reconsider the existing quality standards for glass and to replace destructive 4-point bending test and fragmentation test by SCALP non-destructive residual stress measurement in glass panels. Many publications support of this proposal [1–3].

6.2 Stress inhomogeneity (Paper II)

In Paper II we investigated the stress inhomogeneity in thermally tempered glass plates. For this purpose polariscope SCALP-04 was used. The aim was to measure stress variation correlation to tempering cooling air jet positions.

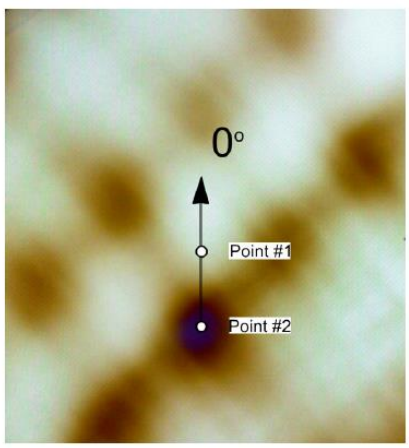

Figure 6.2 Interference pattern in circular polariscope of thermally tempered glass plate.

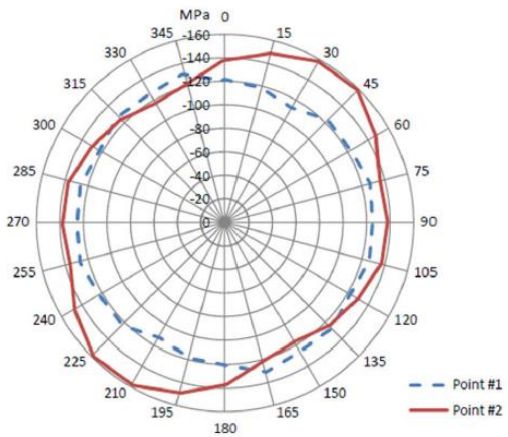

Figure 6.3 Directional variation of surface stress at points 1 and 2 of the glass plate shown in Figure 6.2.

Figure 6.2 shows the fringe pattern in a transmitted light polariscope of the middle part of a tempered glass plate. Figure 6.3 depicts the surface stress ellipses for points 1 and 2, the distance between is 12mm. It can be seen that although the distance between points 1 and 2 is very small, the surface stress differs considerably.

SUMMARY AND THE MAIN RESULTS

A new optical method for evaluation of the stress profile in chemically strengthened glass based on confocal detection of scattered laser beam is presented. Confocal microscopy allows scanning within the light beam and collecting Rayleigh-scattered light from a microscopic volume. The obtained spatial intensity profile of the Rayleigh scattering indirectly describes the stress profile in the tempered glass with very high spatial resolution.

Second stress measurement method, intended for stress measurement in chemically strengthened glass, was based on oblique incidence scattered light method. For that method, an algorithm that removes the influence of light ray bending from oblique incidence scattered light method was developed. We present numerical experiments to test this iterative approach which can remove the influence of light ray bending form scattered light tomography. We found that the nature and rate of convergence of the iterative process for compressive and tensile stresses were notably different.

Oblique incidence scattered light non-destructive method is used to investigate the stress build-up in chemically strengthened lithium aluminosilicate glass. We utilize oblique scattered light method to recover a more detailed stress profile around the knee. The main motivation of the work was to characterize and optimize the development of the knee-shaped breaking point in stress profile in lithium aluminosilicate glass using one-step strengthening in a mixture of KNO_3+$NaNO_3$ molten salt bath. In the industry, it is still common using a two-step process to build such a stress profile. Single-step strengthening will simplify the process as well as save the cost.

A significant find was that the iterative algorithm that was first tested in simulations also removed the influence from experimentally measured stress profiles. The iterative scheme was tested for the same purpose on experimentally measured stress profiles of chemically strengthened lithium aluminosilicate. It was concluded that stress equilibrium error was reduced by using this iterative algorithm to calculate stress form experimental optical retardation data.

We also examined tempered glass plates of various thermal treatments. A linear correlation was found between surface compression measured with oblique incidence scattered light method and breaking strength measured with traditional four-point bending tests. Stress inhomogeneity was also investigated. It has been shown that surface compression of thermally tempered glass panels may vary both locally (at a distance equal to the distance between the cooling jets) and globally, i.e., stresses near the edges and corners of the panels differ significantly from the stresses in the middle part of the panels.

SUMMARY IN ESTONIAN

Jääkpingete sügavusprofiili mõõtmine keemiliselt tugevdatud ja termiliselt karastatud klaasplaatides kasutades hajunud valguse meetodit

Arendati välja konfokaalmikroskoopial ja hajunud valguse meetodil põhinev optiline meetod jääkpingete sügavusprofiili mõõtmiseks keemiliselt karastatud klaasis. Konfokaalmikroskoopia võimaldab väga suure ruumilise lahutusega tomograafiliselt sondeerida Rayleigh hajunud valguse intensiivsuse jaotust ja sellest arvutada jääkpingete profiil karastatud klaasis.

Teine metoodika, mida kasutati pingeprofiilide mõõtmiseks keemiliselt karastatud klaasis põhines klaasplaadile hajunud valguse meetodil kus pealelangev valgus oli kaldu uuritava klaasplaadiga. Selle metoodika jaoks arendati välja valguse paindumise mõju eemaldav iteratiivne algoritm. Algoritmi testimisel leiti, et selle konvergeerumiskiirus sõltus sellest kas klaasi pinnal olid surve- või tõmbepinged.

Hajunud valguse meetodiga uuriti mittepurustavalt pingeprofiile liitium aluminosilikaat klaasis. Uue metoodikaga suudeti mõõta pingprofiili iseäralikke karakteristikuid, mida polnud varem kasutuses olnud meetoditega võimalik mõõta. Uuritavad klaasid olid valmistatud ühekordse karastamisetapiga KNO_3+$NaNO_3$ soolade segus.

Olulise tulemusena näidati, et simulatsioonides valguse paindumise mõju edukalt eemaldav algoritm toimis ka eksperimentaalsete pingeprofiilide peal. Selle kinnituseks oli survepingete ja tõmbepingete vahelise tasakaalu oluline paranemine optilise käiguvahe jaotusest arvutatud pingeprofiilis. Välja arendatud algoritm on seega piisavalt testitud, et kasutada seda Eesti firma GlasStress OÜ poolt toodetavas polariskoobis SCAPL-05.

Samuti näidati termiliselt karastatud klaasplaatide pinnasurvepingete (mõõtes selle hajunud valguse meetodil) ja purustamispinge vahelist lineaarset korrelatsiooni. Sama metoodikaga uuriti ka pingete ebaühtlust termiliselt karastatud klaasides. Näidati, et pinnapinged erinevad oluliselt sõltuvalt uuritavast asukohast.

ACKNOWLEDGEMENTS

Firstly, I would like to thank my supervisor, Professor Jaak Kikas, for patiently supervising me from the start of my bachelor's studies to the end of my Ph. D. I also thank my second supervisor Eric Tkaczyk, who got involved at later stages of my work. This study was mentored by Acad. Hillar Aben, whom I am very thankful. I truly appreciate Johan Anton's support to my research effort. Mart Paemurru was always a skilled experimenter with SCALP and AP (let us point out that he is also the one who assembles most of the both polariscopes in the first place). Andreas Valdmann has been amazingly productive co-author and a good colleague whom to discuss scientific problems. Valter Kiisk was always ready to help out when difficult questions appeared in papers. I thank my student Priidik Möls who is a talented engineer with good SolidWorks skills. I also would like to thank my Japanese colleague Takashi Murata for producing LAS glass samples.

I thank Johanna Rosenvald for being a good friend and being always concerned what I am up to. I thank Kelly and little rabbit (jänkupoiss) for motivating me. This work has been partially supported by Enterprise Estonia, graduate school „Functional materials and technologies," receiving funding from the European Social Fund under project 1.2.0401.09-0079 in Estonia, by European Social Fund's Doctoral Studies and Internationalisation Programme DoRa, and the Kristjan Jaak scholarships from the Archimedes foundation. This research was a part of the project "REMARK" (Estonian Ministry of Education and Research contract 10.1-9/12/380), which was supported by the European Union through the European Regional Development Fund.

REFERENCES

1. Schiavonato M, Mognato E, Redner A. S. Stress measurement, fragmentation and mechanical strength. *Proc. International Conference "Glass Processing Days 2005. Tampere, Finland.* 2005;92–95.
2. Carré H, Daudeville L. Analysis of residual stresses and of the load-bearing capacity of tempered glass plates. *Proc. 4th European Conference on Residual Stresses. Cluny en Bourgogne.* 1996;377–386.
3. Dubru M, Nugue JC, Lummen G. Toughened glass: mechanical properties and EN12600 behaviour. *Proc. International Conference Glass Processing Days.* 2005, 1–5.
4. Maxwell JC. On the equilibrium of elastic solids. *Trans Roy Soc Edinburgh* 1853; 20(1): 87–120.
5. Weller R. Three dimensional photoelasticity using scattered light. *J Appl Phys.* 1941;12(8):610–616.
6. Aben H, Lochegnies D, Chen Y, Anton J, Paemurru M, Õis M. A new approach to edge stress measurement in tempered glass panels. *Experimental Mechanics.* 2015; 55 (2):483−486.
7. Bateson S, Hunt J, Dalby DA, Sinha NK. Stress measurements in tempered glass by scattered light method with a laser source. *Bull Am Ceram Soc.* 1966;45(2):193–198.
8. Cheng YF. An investigation of residual stresses in tempered glass plates of aircraft windshields. *J Aircraft.* 1969;6(2):156–9.
9. Cheng YF. A dual-observation method for determining photoelastic parameter in scattered light. *Experimental Mechanics.* 1969;7(3):140–144.
10. Bradshaw W. Stress profile determination in chemically strengthened glass using scattered light. *J Mater Sci.* 1978;14(12)**:**2981–88.
11. Kishii, T.; Takashio, H.: Scattered light photoelasticity of glass by argon ion laser. *J Ceram Soc Japan.* 1972;4, 137-141.
12. Colombotto A, Ravarino S, Muzü L. Optical methods for stress measurement in glass plates. *Strength of inorganic glass. NATO Conference VI, Materials Science 11. New York*. 1985;591–596.
13. Weissman R, Dürkop D. A novel method for measuring stresse in flat glass. *Proc. XV Internat. Congr. Glass, Leningrad 1989, Leningrad.* 1989;3b:217–221.
14. Shepard CL, Cannon BD, Kahleel MA. Measurement of internal stress in glass article. *J Am Ceram Soc.* 2003;86(8):1353–59.
15. Anton J, Aben H. (2003) A compact scattered light polariscope for residual stress measurement in glass. *Glass Processing Days: Conf Proc.* 2003;86–88.
16. Tennakoon S. Novel method for stress inspection of temered of thermally strengthened glass. *73rd Conference on Glass Problems. The American Ceramic Society.* 2013;259–266.
17. Dolovich AT, Wang Z, Gladwell GML. An iterative approach to curved ray reconstruction of birefringent fields. *Opt Lasers Eng*. 1995;22:347–372.
18. Dolovich AT, Gladwell GML. Convergence criteria for iterative schemes in holographic interferometry and the tomography of strongly refracting objects. *Appl Opt.* 1989;28:4411–4418.
19. Lira IH, Vest CM. Refraction correction in holographic interferometry and tomography of transparent objects. *Appl Opt.* 1987;26:3919–28.

20. Acosta E, Vazquez D, Smith G, Garner L. Tomographic method for measurement of the gradient refractive index of the crystalline lens. II. The rotationally symmetrical lens. *Journal of the Optical Society of America A: Optics and Image Science, and Vision.* 2006;23 (10):2551–65.
21. Bokshtein M F. On the resolving power of polarizing system for stress investigations. *Zhurnal Tekhnischeskoi Fiziki*. 1949;19:1103–1109. (in Russian)
22. Hecken FW, Pindera JT. Basic theory and experimental techniques of the strain-gradient method. *Experimental Mechanics.* 1987;27:314–327.
23. Aben H, Krasnowski BR, Pindera JT. Nonrectilinear light propagation in integrated photoelasticity of axisymmetric bodies. *Transactions of the Canadian Society for Mechanical Engineering*. 1984;8(4):195–200.
24. Pagnotta L, Poggialini P. Measurement of residual stresses in optical fiber preforms. *Experimental Mechanics.* 2002;43(1):69–76.
25. Acloque P, Guillemet C. Method for photoelastic measurement of stresses "in equilibrium in the thickness" of a plate. (particular cases of toughened glass and bent glass). *Verres Refract*. 1960:14:3-10.
26. Indenbom VL. On the Theory of the Tempering of Glass. Zhurnal Tekhnicheskoi Fiziki, 1954;24:925–928
27. Narayanaswamy OS. A model of structural relaxation in glass. *J Am Ceram Soc.* 1971:54(10):491–498
28. Shen J, Green DJ.Variable-temperature ion-exchanged engineered stress profile glasses. *J Am Cer Soc.* 2004;86(11):1979–81.
29. Wang HF, Xing GZ, Wang XY, Zhang LL, Zhang L (2014) Chemically strengthened protection glasses for the applications of space solar cells. AIP Advances 4:047133
30. Mazzoldi P, Carturan S, Quaranta A, Sada C, Sglavo VM (2013) Ion exchange process, evolution and applications. Rivista del Nuovo Cimento 36(9):397–460
31. Salmaso B, Civitani M, Brissolari C, Basso S, Ghigo M, Pareschi G, Spiga D, Proserpio L, Suppiger Y Development of mirrors made of chemically tempered glass foils for future X-ray telescopes. *Experimental Astronomy*. 2015;39(3)527–545
33. Varshneya AK, Spinelli IM. High-strength, large-case-depth chemically strengthened lithium aluminosilicate glass. *Am Ceram Soc Bull*. 2009;88(5):213–20.
34. Jannotti P, Subhash G, Ifju P, Kreski PK, Varshneya AK. Photoelastic measurement of high stress profiles in ion-exchanged glass. *Int J Appl Glass Sci.* 2011;2(4):275–281.
35. Jannotti P, Subhash G, Varshneya AK. Ball impact response of unstrengthened and chemically strengthened glass bars. J Am Ceram Soc. 2014;97(1):189–197.
36. Jannotti P, Subhash G, Ifju P, Kreski PK, Varshneya AK. Influence of ultra-high residual compressive stress on the static and dynamic indentation response of a chemically strengthened glass. *J Eur Ceram Soc*. 2012;32(8):1551–1559.
37. Marusak FJ. Double ion exchange method for making glass article. Patent US3410673 (12. Nov 1968)
38. Saunders AE, Kubichan RE. Strengthening glass by multiple alkali ion exchange. Patent US3433611 (18. Mar 1969)
39. Piksarv et al. Integrated single- and two –photon light sheet micriscoply using accelerating beam. *Scientific Reports.* 2014;7:1435
40. Nissle TR, Babcock CL. Stress-optical coefficient as related to glass composition. *J Am Ceram Soc*. 1973;56:596–598.
41. Matusita *et al*. Photoelastic effects in silicate glasses. *J Am Ceram Soc*. 1984;67: 700–704.

42. Smedskjaer M, S. A. Saxton S, Ellison A, Mauro JC, "Photoelastic response of alkaline earth aluminosilicate glasses," *Opt Letters.* 2012;37:293–295.
43. Fourney ME., Chang BW. Scattered light and fluorescent photomechanics. *Proc Soc Photo- Opt Instrum Eng.* 1987;814:174–183.
44. Stewart OJ, Young DW. The action of molten lithium salts on glass. *J Am Chem Soc*. 1935;57(4):695–698.
45. Ernsberger F. On the nature of cracks on the surface of glass. *Glass and Ceramics.* 1960;17 (12):659.
46. Garfinkel HM, King CB. Ion concentration and stress in a chemically tempered glass. *J Am Cer Soc.* 1970;53(12):686–91.
47. Varshneya AK. Kinetics of ion exchange in glasses. *J Non-Cryst Sol*. 1975;19:355–365.
48. Sglavo VM. Chemical strengthening of soda lime silicate float glas: effect of small differences in in the KNO_3 bath. *Int J Appl Glass Sci.* 2014;6(1):72–82.
49. Albert J, Yip GI. Stress-induced induced index change for K^+-Na^+ ion exchange in glass. *Electron Lett.* 1987;23(14):737–738.
50. Brandenburg A. Stress in ion-exchanged waveguides. *J Lightwave Technol.* 1986: 4(10):1580–1583.
51. Inaba S, Ogami S, Orihara S, Orihara Y. Non-destructive stress measurement in double ion-exchanged glass using optical guided-waves and scattered light. *J Ceram Soc Japan.* 2017;125(11):814-820.
52. Nordberg et al. Strengthening by ion exchange. *J Am Cer Soc.* 1964;47(5):215–219.
53. Nie et al. Dynamic ring-on-ring equibiaxial flexural strength of borosilicate glass. *Int J Appl Ceram Technol*. 2010;7(5):616–624.
54. Brodland GW, Dolovich AT. Curved-ray technique to measure stress profile in tempered glass. *Opt Eng.* 2000;39(9):2501-5.

PUBLICATIONS

CURRICULUM VITAE

Name: Siim Hödemann
Date of birth: March 22, 1982, Võru, Estonia
Citizenship: Estonian
Address: Wilhelm Ostwald Str.1, 50411, Tartu, Estonia,
E-mail: siimh@ut.ee

Education:

2001	Võru Kreutzwald's high school
2005	University of Tartu B. Sc in materials science
2007	University of Tartu M. Sc. in materials science

Professional career:

2007–2015	University of Tartu, Institute of Physics, engineer
2015	University of Tartu, Institute of Physics, specialist

Awarded research projects:

2014	Estonian Enterprise project "Numerical simulations to take light ray bending into account for SCALP-05, that is specifically intended for stress profile measurement in chemically tempered glass (1.11.2014−31.08.2015)"; project was fulfilled together with Andreas Valdmann. Partially funded by GlassStress Ltd.
2015–2017	Scholarship of teaching and learning (SoTL) project "Adaptation of Olympiad-style experimental problems (from international physics Olympiads) for second year university experimental courses on electricity-magnetism and optics"
2016	Esonian Enterprise project "Development of algorithms to remove the influence of light ray bending from automatic polariscope AP-07 that is intended to measure stress in axi-symmetric chemically strengthened glass (1.02.2016−31.08. 2017)"; project was fulfilled together with Andreas Valdmann. Partially funded by GlassStress Ltd.

List of Publications:

Related to the Ph. D. thesis:

1) H. Aben, J. Anton, A. Errapart, S. Hödemann, J. Kikas, H. Klaassen and Marko Lamp. "On non-destructive residual stress measurement in glass panels," *Estonian Journal of Engineering*, **16**(2):140–143 (2010)
2) J. Anton, A. Errapart, M. Paemurru, Dominique Lochegnies, Siim Hödemann and H. Aben. "On the inhomogeneity of stresses in tempered glass panels," *Estonian Journal of Engineering* **18**(1):3–11 (2012)
3) S. Hödemann, P. Möls, J. Kikas and J. Anton. "Scattered laser light fringe patterns for stress profile measurement in tempered glass plates," *Glass*

Technology: European Journal of Glass Science and Technology **55**(3):90–95 (2014)

4) S. Hödemann, P. Möls, V. Kiisk, T. Murata, R. Saar, J. Kikas. "Confocal determination of Rayleigh scattering for residual stress measurement in chemically tempered glass," *Journal of Applied Physics* **118**:243103 (2015)
5) S. Hödemann, A. Valdmann, J. Anton, T. Murata. "Gradient scattered light method for non-destructive stress profile measurement in chemically strengthened glass," *Journal of Materials Science* **51**:5962–78 (2016)
6) S. Hödemann, A. Valdmann, V. Kiisk. "An iterative approach to remove the influence of light ray bending from micron-scale scattered light tomography," *Optics and Lasers in Engineering* **91**:30–40 (2017)

International conference presentations related to the Ph. D. thesis:

2009 On complete non-destructive residual stress measurement in architectural glass panels and automotive glazing. Glass Performance Days, Tampere, Finland, 12–15 June 2015 (co-author of presentation, participating in conference)

2010 On the destructive and non-destructive assessment of strength of thermally toughened glass panels. Annual Meeting Society of Glass Science and Technology, England, University of Cambridge, 8–10. Sept. 2010 (oral presentation)

2011 Effects of ray bending in scattered light photoelasticity for tempered and annealed glass plates. 8th International Conference on Advances in Experimental Mechanics: Integrating Simulation and Experimentation for Validation (BSSM 2011), Scotland, Edinburgh, 7–9. Sept. 2011 (oral presentation)

2012 On the precision of scattered light photoelasticity for tempered glass plates. OptiMess 2012, Belgium, Antwerp, 4–5. April 2012 (oral presentation)

Supervised theses:

2016 Artur Pata, BSc in Materials Science "Straw bale walls as passive house envelope in the Estonian climate"

2015 Priidik Möls, MSc thesis in Materials Science "Confocal detection of Rayleigh scattering for stress profile measurement in chemically strengthened glass"

2013 Priidik Möls, BSc in Materials Science "Development of methods for residual stress measurement in strengthened glasses"

Teaching:

2018– "(LTFY.02.002) Classes and Technologies of Materials, Ceramics and Glasses (3 ECTS)" lecturer of 50% of the lecutres of the courese (the part of glasses).

2017– "(LTFY.01.007) Electricity and Magnetism (6 ECTS)" supervisor of problem solving seminar.

2017–2018 "(LTFY.02.003) Review Course of Materials Science, (6 ECTS)" lecturer of 12 lectures on optical properites and optical meterials.
2011–2017 "(LTFY.02.039) Electrical Properites of Matter, (6 ECTS)" supervisor of problem solving seminar.
2012– "(LTFY.02.007) Practical Works in Materials Physics. Optics (3 ECTS)" co-supervisor of experimental lab.
2006– "LTFY.02.007) Practical Works in Materials Physics. Electricity and Magnetism (3 ECTS)" supervisor of experimental lab

Public and social activities:
Member of re-enactment club "Front-Line" and history and war veteran's support club "Wiking-Narva".

Hobbies: realistic drawing with charcoal and judo.

ELULOOKIRJELDUS

Nimi: Siim Hödemann
Sünniaeg: 22. märts 1982, Võru, Eesti
Kodakondsus: Eesti
Aadress: Wilhelm Ostwaldi 1, 50411, Tartu, Estonia
E-post: siimh@ut.ee

Haridustee:

2001 Võru Kreutzwaldi Gümnaasium
2005 Tartu Ülikool B. Sc. materjaliteaduses
2007 Tartu Ülikool M. Sc. füüsikalises materjalitehnoloogias

Töökogemus:

2007–2015 Tartu Ülikool, Füüsika Instituut, insener
2015 Tartu Ülikool, Füüsika Instituut, spetsialist

Uurimisprojektid:

2014 Ettevõtluse Arenduse Sihtasutuse (EAS) projekt "Numbrilised arvutused valguse paindumise mõju eemaldamiseks hajunud valguse polariskoobis SCALP-05" (1.11.2014−31.08.2015)"; projekti täideti koos Andreas Valdmanniga. Projekti kaasfinantseeris GlassStress OÜ.

2015–2017 Õpetamise ja õppimise uurimise projekt "Olümpiaadi-stiilis eksperimentide kohandamine bakalaureuseõppe praktikumide jaoks"

2016 EAS projekt "Valguse paindumise mõju eemaldamine automaatpolariskoobiga AP-07 mõõdetud keemiliselt karastatud telgsümmeetriliste klaasobjektide jääkpingete profiilidest. (1.02. 2016−31.08.2017)"; projekti täideti koos Andreas Valdmanniga. Projekti kaasfinantseeris GlassStress OÜ.

Teaduspublikatsioonide loetelu:

1) H. Aben, J. Anton, A. Errapart, S. Hödemann, J. Kikas, H. Klaassen and Marko Lamp. "On non-destructive residual stress measurement in glass panels," *Estonian Journal of Engineering*, **16**(2):140–143 (2010)
2) J. Anton, A. Errapart, M. Paemurru, Dominique Lochegnies, Siim Hödemann and H. Aben. "On the inhomogeneity of stresses in tempered glass panels," *Estonian Journal of Engineering* **18**(1):3–11 (2012)
3) S. Hödemann, P. Möls, J. Kikas and J. Anton. "Scattered laser light fringe patterns for stress profile measurement in tempered glass plates," *Glass Technology: European Journal of Glass Science and Technology* **55**(3):90–95 (2014)

4) S. Hödemann, P. Möls, V. Kiisk, T. Murata, R. Saar, J. Kikas. "Confocal determination of Rayleigh scattering for residual stress measurement in chemically tempered glass," *Journal of Applied Physics* **118**:243103 (2015)
5) S. Hödemann , A. Valdmann, J. Anton, T. Murata. "Gradient scattered light method for non-destructive stress profile measurement in chemically strengthened glass," *Journal of Materials Science* **51**:5962–78 (2016)
6) S. Hödemann, A. Valdmann, V. Kiisk. "An iterative approach to remove the influence of light ray bending from micron-scale scattered light tomography," *Optics and Lasers in Engineering* **91**:30–40 (2017)

Osalemine rahvusvahelistel teaduskonverentsidel:

2009 On complete non-destructive residual stress measurement in architectural glass panels and automotive glazing. Glass Performance Days, Tampere, Soome, 12–15 juuni 2015 (ettekande kaasautor, osalemine konverentsil)
2010 On the destructive and non-destructive assessment of strength of thermally toughened glass panels. Annual Meeting Society of Glass Science and Technology, Inglismaa, Cambridge'i Ülikool, 8–10. sept. 2010 (suuline ettekanne)
2011 Effects of ray bending in scattered light photoelasticity for tempered and annealed glass plates. 8th International Conference on Advances in Experimental Mechanics: Integrating Simulation and Experimentation for Validation (BSSM 2011), Šotimaa, Edinburgh, 7–9. Sept. 2011 (suuline ettekanne)
2012 On the precision of scattered light photoelasticity for tempered glass plates. OptiMess 2012, Belgia, Antwerpen, 4–5. aprill 2012 (suuline ettkanne)

Juhendatud bakalaureusetööd:

2016 Artur Pata, B. Sc. materjaliteaduses „Põhupakkseinte sobivus passiivmaja välispiireteks Eesti kliimas"
2015 Priidik Möls, M. Sc. materjaliteaduses „Jääkpingete uurimine konfokaalse hajunud valguse meetodiga liitium-aluminosilikaatklaasis"
2013 Priidik Möls, B. Sc. materjaliteaduses „Jääkpingete mõõtmise metoodika arendamine karastatud klaaside jaoks"

Õpetamine:

2018– "(LTFY.02.002) Materjaliklassid ja Tehnoloogiad, Keraamika ja Klaasid (3 EAP)" lektor
2017– "(LTFY.01.007) Elekter ja Magnetism (6 EAP)" ülesannete lahendamise seminar
2017–2018 "(LTFY.02.003) Materjaliteaduse ülevaatekursus, (6 EAP)" lektor, 12 loengut
2011–2017 "(LTFY.02.039) Materjalide elektrilised omadused, (6 EAP)" ülesannete lahendamise seminar

2012– “(LTFY.02.007) Materjalifüüsika praktikum. Optika (3 EAP)” praktikumi juhendaja

2006– “(LTFY.02.007) Materjalifüüsika praktikum. Elekter ja Magnetism (3 EAP)” praktikumi juhendaja

Hobid: Ajalooliste lahingute taaslavastamine klubis “Front-Line”. Teise maailmasõja eesti veteranide toetusklubi “Wiking-Narva” liige. Joonistamine ja judo.

DISSERTATIONES SCIENTIAE MATERIALIS UNIVERSITATIS TARTUENSIS

1. **Martin Järvekülg.** Tubular microstructures by Hf-, Zr- and Ti-butoxide gel sheet rolling. Tartu, 2011, 112 p.
2. **Sergei Vlassov.** Investigation of nanoscale interactions and mechanical properties of nanostructures using quartz tuning fork based real-time measurements. Tartu, 2011, 171 p.
3. **Margus Kodu.** Pulsed Laser Deposition of Magnesium Oxide and Barium Ternary Oxides for Plasma Display Protective Layers. Tartu, 2011, 89 p.
4. **Rainer Pärna.** Surface studies of some oxide films. Tartu, 2011, 129 p.
5. **Jevgeni Šulga**. Self-assembly and interaction of nanostructures. Tartu, 2011, 114 p.
6. **Wojciech Kuznik.** Quantum-chemical computer simulations of the linear and non-linear optical properties of pyrazoloquinoline and dicyanopyrazine derivatives. Tartu, 2012, 89 p.
7. **Leonid Dorogin.** Structural and tribological properties of zero- and one-dimensional nanocrystals. Tartu, 2012, 193 p.
8. **Viljar Palmre.** Fabrication and characterization of microporous carbon-based electroactive polymer actuators. Tartu, 2012, 99 p.
9. **Madis Paalo**. Synthesis of CNT-metal oxide nanocomposites: sol-gel process, rheology, structural and functional properties. Tartu, 2014, 175 p.
10. **Raul Välbe.** Developement of ionic liquid composites by sol-gel method for elaboration of industrial nano- and microstructures. Tartu, 2014, 97 p.
11. **Urmas Joost.** Impurity and preparation dependent properties of titania thin films. Tartu, 2014, 155 p.
12. **Madis Umalas**. Application of sol-gel technology for production of ceramic nanocomposites and functional coatings. Tartu, 2015, 136 p.
13. **Elena Samsonova.** Energy transfer probe as a tool to study morphological and structural origins of fluorescence quenching in rare-earth doped nanophosphors. Tartu, 2015, 114 p.
14. **Jay Mondal.** Novel Corrosion Protective Nanostructured Composite Coatings. Tartu, 2016, 104 p.
15. **Kathriin Utt.** Metal oxide mesostructures for optical applications. Tartu, 2016, 88 p.
16. **Kaido Siimon.** Electrospun gelatin cross-linked by glucose. Tartu, 2016, 84 p.
17. **Marko Part.** Combined three-dimensional sol-gel structures and atomic layer deposited thin films. Tartu, 2017, 162 p.
18. **Pejman Rasti.** Analysis of Remote Sensing Image Super Resolution using Fluid Lenses. Tartu, 2017, 188 p.
19. **Ivo Romet.** Recombination luminescence of doped borates: origin and application prospects in dosimetry. Tartu, 2017, 111 p.

20. **Vladimir I. Kondratiev.** Processing and characterization of transparent electrode materials. Tartu, 2017, 111 p.
21. **Taivo Jõgiaas**. Mechanical properties of atomic layer deposited thin films and nanocomposites. Tartu, 2017, 125 p.
22. **Lauri Aarik**. Atomic layer deposition and characterization of thin oxide films for application in protective coatings. Tartu, 2017, 180 p.
23. **Triin Kangur.** Preparation and functional properties of stochastic micro-structured sol-gel silica materials. Tartu, 2018, 96 p.
24. **Marta Berholts.** Fragmentation of ionic and hydrogen-bonded molecules induced by synchrotron radiation. Tartu, 2018, 126 p.
25. **Priit Priimägi.** Development and optimization of 3D-microbatteries. Tartu, 2018, 118 p.